An overview of pathways of ENSO influence on the extra-tropics

In-Sik Kang

Second Institute of Oceanography, China

Content

- Review of those earlier papers, provided an original concept and theory for the extratropical teleconnection associated with ENSO.
- Question on the PNA; internal vs forced modes
- Issues on climate model simulations of the teleconnection

Review of earlier papers

- Bjerknes (1966, 1969) “ENSO” and “Teleconnection”
- Hoskins and Karloy (1981) “Rossby Wave ray theory”
- Simmons et al. (1983) “Regional barotropic instability”
- Held et al. (1989) “Transient forcing”
- Stratospheric path way

MONTHLY WEATHER REVIEW
VOLUME 97, NUMBER 3
MARCH 1969

UDC 551.513:551.509.338:551.465.6(265)(267)

ATMOSPHERIC TELECONNECTIONS FROM THE EQUATORIAL PACIFIC [1]

J. BJERKNES

Department of Meteorology, University of California, Los Angeles, Calif.

ABSTRACT

The "high index" response of the northeast Pacific westerlies to big positive anomalies of equatorial sea temperature, observed in the winter of 1957–58, has been found to repeat during the major equatorial sea temperature maxima in the winters of 1963–64 and 1965–66. The 1963 positive temperature anomaly started early enough to exert the analogous effect on the atmosphere of the south Indian Ocean during its winter season.

The maxima of the sea temperature in the eastern and central equatorial Pacific occur as a result of anomalous weakening of the trade winds of the Southern Hemisphere with inherent weakening of the equatorial upwelling. These anomalies are shown to be closely tied to the "Southern Oscillation" of Sir Gilbert Walker.

Bjerknes (1966, 1969) "ENSO mechanism" and "Teleconnection"

- Bjerknes wind-thermocline-SST positive feedback for El-Nino formation

- Stronger Jetstream resulted from intensified Hadley circulation can transport more zonal angular momentum to the extratropics, resulting in the stronger westerlies in the NH extratropical Pacific and intensifying the Aleutian low.
- South Indian Ocean teleconnection and Walker circulation changes, associated with the Southern Oscillation (SO).

- El-Nino/Southern Oscillation (ENSO)

The Steady Linear Response of a Spherical Atmosphere to Thermal and Orographic Forcing[1]

BRIAN J. HOSKINS AND DAVID J. KAROLY[2]

U.K. Universities' Atmospheric Modelling Group and Department of Meteorology, University of Reading, RG6 2AU England

(Manuscript received 21 November 1980, in final form 23 February 1981)

ABSTRACT

Motivated by some results from barotropic models, a linearized steady-state five-layer baroclinic model is used to study the response of a spherical atmosphere to thermal and orographic forcing. At low levels the significant perturbations are confined to the neighborhood of the source and for midlatitude thermal forcing these perturbations are crucially dependent on the vertical distribution of the source. In the upper troposphere the sources generate wavetrains which are very similar to those given by barotropic models. For a low-latitude source, long wavelengths propagate strongly polewards as well as eastwards. Shorter wavelengths are trapped equatorward of the poleward flank of the jet, resulting in a split of the wavetrains at this latitude. Using reasonable dissipation magnitudes, the easiest way to produce an appreciable response in middle and high latitudes is by subtropical forcing. These results suggest an explanation for the shapes of patterns described in observational studies.

The theory for waves propagating in a slowly varying medium is applied to Rossby waves propagating in a barotropic atmosphere. The slow variation of the medium is associated with the sphericity of the domain and the latitudinal structure of the zonal wind. Rays along which wave activity propagates, the speeds of propagation, and the amplitudes and phases along these rays are determined for a constant angular velocity basic flow as well as a more realistic jet flow. They agree well with the observational and numerical model results and give a simple interpretation of them.

Kang, JAS 1990

Influence of Zonal mean flow Change
On Stationary wave fluctuations

$\bar{u}_2$ but with the same topography is shown in Fig. 6. In this figure, the downstream anomaly forced by the Himalaya mountains is particularly pronounced in the Pacific sector, but in the western hemisphere the mountain induced anomaly is fairly weak compared with the GCM counterpart. Although the low in the mid-Pacific shown in Fig. 4 is still shifted northwestward, the general pattern of the wave train in the Pacific and North American sector is similar to the GCM counterpart and that shown in Fig. 5. This result suggests that a large fraction of the anomalous eddy streamfunction in the Pacific and North American region is a result of differences in the wave trains induced by the same mountain but propagated through different zonal mean flows.

5. Idealized case

In section 4, it is shown that two different basic states produce different wave trains for the same atmospheric forcing, and consequently that the change of the zonal mean flow itself can cause significant anomalous circulation in the atmosphere. We now investigate how the horizontal structure of the wave train is determined by the basic states, $\bar{u}_1$ and $\bar{u}_2$, by examining the Rossby wave ray theory (e.g., Hoskins and Karoly 1981; Held 1983) and the responses of the linear barotropic model to idealized vorticity sources.

a. Theoretical preliminary

In the Mercator projection of the sphere, the linearized vorticity equation (1) for a steady state can be written as

$$\bar{u}_M \frac{\partial}{\partial x} \nabla^2 \Psi^* + \beta_M \frac{\partial \Psi^*}{\partial x} = 0 \qquad (2)$$

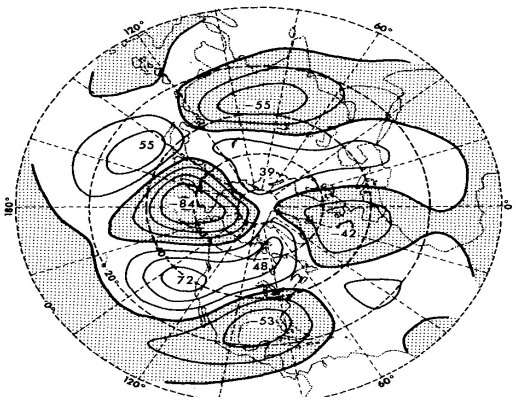

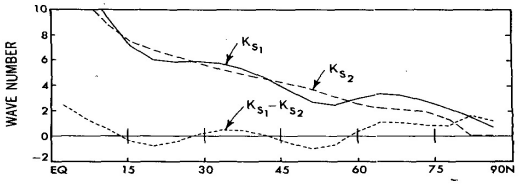

FIG. 7. Meridional structures of the stationary wavenumber K_S multiplied by the earth's radius for the zonal mean flows $\bar{u}_1$ and $\bar{u}_2$.

where $x = a\lambda$, $y = a \ln[(1 + \sin\phi)/\cos\phi]$, and $\bar{u}_M = \bar{u}/\cos\phi$, $\beta_M = \dfrac{d}{dy}(f - d\bar{u}/dy)$. Introducing a wave solution $\Psi = \tilde{\Psi}(y)e^{ikx}$ into Eq. (2), we obtain the following equation.

$$\frac{d^2\tilde{\Psi}}{dy^2} + (K_S^2 - k^2)\tilde{\Psi} = 0 \qquad (3)$$

where $K_S = (\beta_M/\bar{u}_M)^{1/2}$ is the stationary wavenumber. Equation (3) gives a criterion for meridional propagation of the wave. If $K_S > k$ the wave can propagate meridionally, but at latitudes where $K_S < k$ it is exponentially damped. In the above the stationary wavenumber is solely determined by the meridional structure of the zonal mean flow, and the ray amplitude of wavenumber k depends on the magnitude of forcing projected onto the wavenumber space k and the medium through which the wave propagates. The WKB theory tells that

$$\Psi \approx \frac{1}{\sqrt{l}} \exp[i(kx + \int^y l\,dy)] \qquad (4)$$

where $l^2 = K_S^2 - k^2$. Thus the wave amplitude is proportional to $l^{-1/2}$, and at the turning latitude where $K_S = k$, the amplitude becomes infinity. However, this formula breaks down near the turning point, where the WKB solution must be matched to the decaying solution on the other side and the solution is expressed in terms of Airy functions. But the amplitude still reaches its maximum near the turning point. Overall, the meridional structure of K_S is the *only* factor that determines the propagation characteristics and amplitude of the wave forced by a given forcing.

The meridional structures of K_S multiplying by the earth's radius for the zonal mean flows $\bar{u}_1$ and $\bar{u}_2$ denoted by K_{S_1} and K_{S_2}, respectively, are shown in Fig. 7. The major differences between the two K_S curves are in middle and high latitudes; K_{S_2} is bigger than K_{S_1} in midlatitudes while the reverse is true in high latitudes. For instance, when a planetary-scale wave (e.g., of wavenumber 3) is incident from the subtropics, the wave can propagate to midlatitudes in both basic

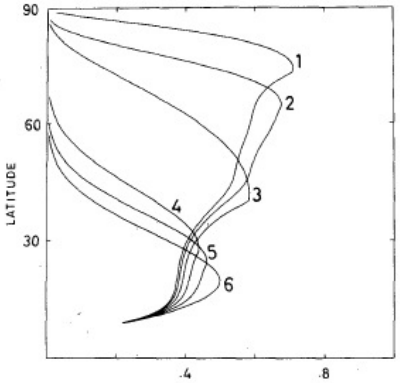

FIG. 14. Amplitudes of the extrema on the rays for different zonal wavenumbers on the 300 mb NH zonal flow.

give a good indication of the extrema exhibited in Fig. 1 for the barotropic model[5] and in Fig. 3 for the baroclinic model. The split in the wavetrains with the long waves going polewards and the shorter waves trapped by the northern flank of the jet is very obvious also for the 30° source shown in Fig. 16a. The worst feature when compared with the simple mountain solution in Fig. 4a of Grose and Hoskins (1979) and Fig. 8 in this paper is the zonal extent of the equatorward wavetrain near latitude 20°. Otherwise, agreement is good. The more poleward source in Fig. 16b gives only long waves propagating polewards and equatorwards in agreement with the 45° source shown in Fig. 4.

Any features which are particularly sensitive to the details of the basic flow are probably not of interest, both because of the variation in the equivalent barotropic level in the baroclinic model solutions and because of lack of validity of the WKBJ solution and, in particular, the criterion (5.22). Thus it is of interest to compare the rays and phases for the 15° source using the 500 mb flow (Fig. 17). The main differences are that wavenumber 4 becomes a long poleward propagating wave and the phase separation and thus apparent wavelengths are somewhat smaller. However, the basic pattern is not sensitive.

In Section 3d it was noted that for 1.2 times the basic winter zonal flow there seemed to be a wavenumber 3 resonance. It is interesting that the zonal wavenumber 3 ray shown in Fig. 16 for the basic 300 mb flow does indicate the possibility of such a wave propagating around a significant portion of the hemisphere. For 1.2 times the basic flow this ray does propagate further around, though this is quite sensitive to the smoothing of the flow. The stationary wavenumber K_s is identical with that which is often referred to as the resonant wavenumber. However, apart from the resonant solution mentioned above, resonance plays no part in the theory and model solutions exhibited here.

Finally, we note that the same wave theories can be applied to a free surface barotropic model. The main change is to replace (5.16) by

$$aK_s = [a^2\beta_M/\bar{u}_M - (a^2\Omega^2/gh)\sin^2 2\phi]^{1/2}. \quad (5.29)$$

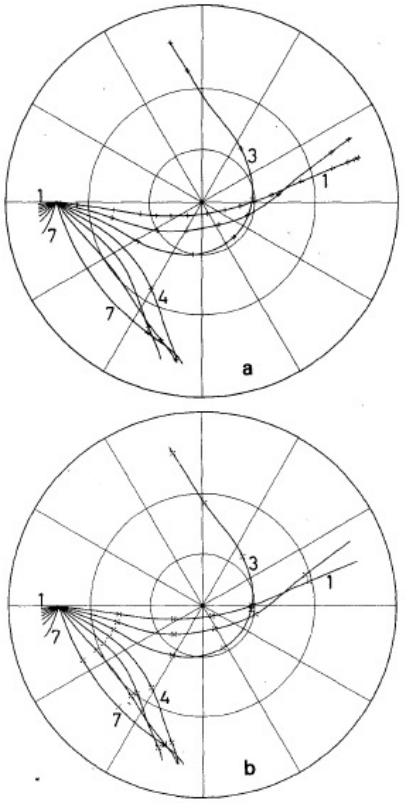

FIG. 15. A 15° source in the NH 300 mb zonal flow (a) mer-

Review of earlier papers

- Bjerknes (1966, 1969) “Teleconnection”

Intensification of westerly momentum associated with intensified Hadley circulation

- Hoskins and Karloy (1981) “Rossby Wave ray theory”
- Simmons et al. (1983) “Regional barotropic instability”
- Held et al. (1989) “Transient forcing”
- Stratospheric path way

Barotropic Wave Propagation and Instability, and Atmospheric Teleconnection Patterns

A. J. SIMMONS

European Centre for Medium Range Weather Forecasts, Shinfield Park, Reading, UK

J. M. WALLACE

Department of Atmospheric Sciences, University of Washington, Seattle, 98195

G. W. BRANSTATOR

National Center for Atmospheric Research,[1] Boulder, CO 80307

(Manuscript received 22 October 1982, in final form 28 January 1983)

ABSTRACT

A global barotropic model, linearized about the 300 mb climatological mean January flow, is perturbed by applying a series of localized forcings distributed throughout the tropics and subtropics. Structures which resemble the observed "Pacific/North American" and "East Atlantic" teleconnection patterns noted by Wallace and Gutzler (1981) tend to recur in the responses. Similar patterns are found to result from the dispersion of isolated initial perturbations placed at a variety of locations in the tropics and midlatitudes.

It is shown that these structures are related to the most rapidly growing mode associated with barotropic instability of the zonally-varying climatological basic state. In the absence of damping, this mode has an *e*-folding time of about a week and a period close to 50 days. In localized regions the instantaneous growth rates can be competitive with those of baroclinic instability. These episodes of rapid local barotropic growth are interspersed with intervals in which the local perturbation relaxes as energy disperses throughout the hemisphere. Some of the less unstable modes exhibit a similar structure and time evolution, while others are spatially fixed and grow exponentially in time, without any periodic modulation.

The dominant processes by which the growing disturbances extract kinetic energy from the basic state can be described in terms of two conversion terms: $-u'v'\partial\bar{u}/\partial y$ and $(v'^2 - u'^2)\partial\bar{u}/\partial x$, where u and v are the velocity components in the zonal (x) and meridional (y) directions, respectively, primes refer to the perturbations, and overbars to the basic state. In the fastest growing mode the dominant process contributing to the growth is found to be the second term, which is largest in the Pacific jet exit region where $u'^2 \gg v'^2$.

Nonlinear initial value calculations for weak damping rates exhibit strong low-frequency oscillations similar in structure and period to those of the most unstable mode. Nonlinear forced solutions show some sensitivity to the polarity of the forcing and they tend to show a larger response in the time average over the first month of the integration than in longer term means. Sensitivity to model resolution, dissipation, and choice of basic state is illustrated by means of selected experiments.

On the basis of these results and recent work by Hoskins *et al.* (1983), it is suggested that much of the low-frequency variability of the Northern Hemisphere wintertime general circulation is associated with disturbances which derive their energy from the basic state through barotropic instability.

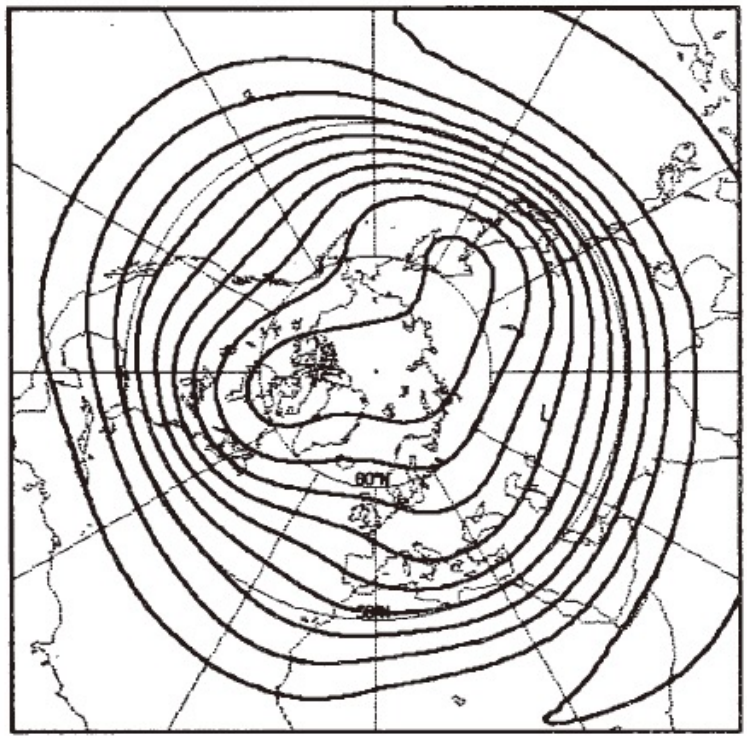

FIG. 2. The climatological-mean 300 mb streamfunction for January. The contour interval is equivalent to a 160 m interval in geopotential height computed by applying the geostrophic approximation at 45°N.

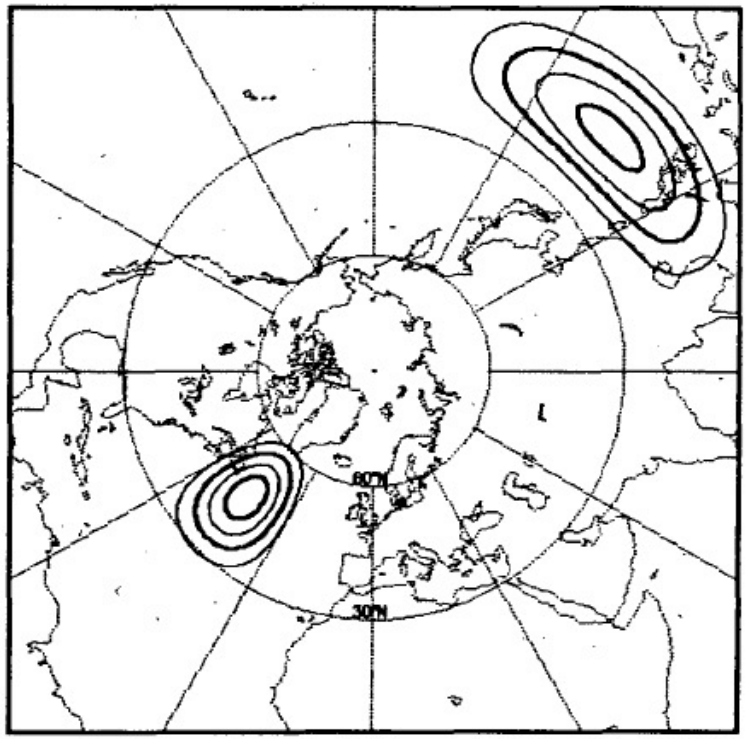

FIG. 3. A sample forcing distribution (centered at 15°N, 135°E) and a sample initial streamfunction perturbation (centered at 45°N, 45°W). The contour interval is one-fifth of the maximum value of each distribution.

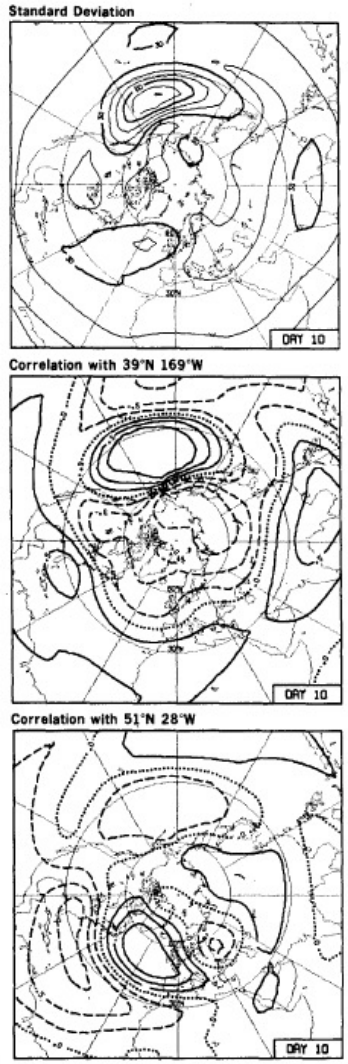

FIG. 4. (a) The standard deviation of the family of forced, perturbation streamfunctions for day 10. The contour interval is equivalent to a 10 m interval for geostrophic geopotential height at 45°N. (b) The corresponding one-point correlation map for the base grid-point 39°N, 169°W. The contour interval is 0.25. Positive contours are drawn with solid lines, negative contours are dashed, and the zero contour is dotted. (c) As in (b), but for the base gridpoint 51°N, 28°W.

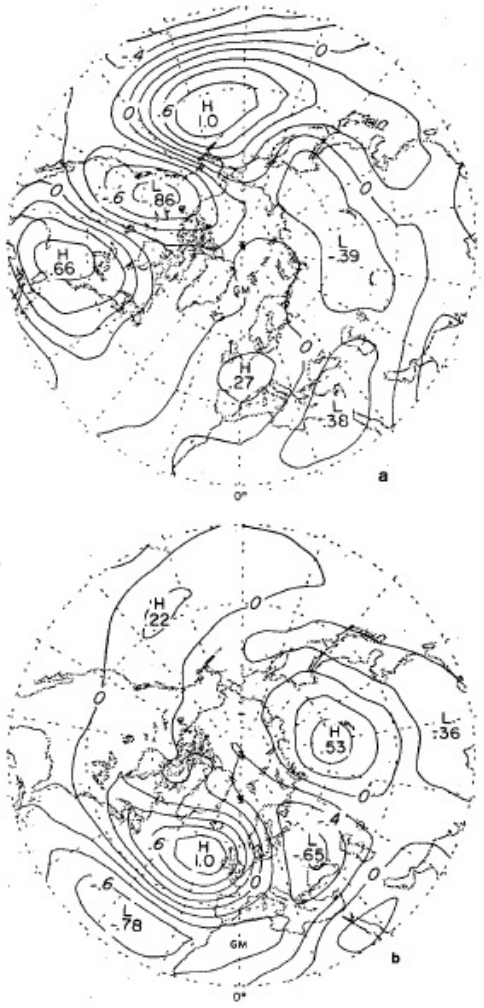

FIG. 1. One-point correlation maps showing the correlation coefficient between 500 mb height at base gridpoints (a) 45°N, 165°W, and (b) 55°N, 20°W, and 500 mb height at other gridpoints in the extratropical Northern Hemisphere. The contour interval is 0.2. From Wallace and Gutzler (1981).

Barotropic Models of the Extratropical Response to El Niño

ISAAC M. HELD

Geophysical Fluid Dynamics Laboratory, Princeton University, Princeton, NJ 08542

IN-SIK KANG

Department of Atmospheric Sciences, Seoul National University, Seoul 151 Korea

(Manuscript received 24 March 1987, in final form 25 June 1987)

ABSTRACT

A series of linear and nonlinear barotropic models are used to interpret the extratropical response to El Niño equatorial surface temperatures as simulated by an atmospheric general circulation model (GCM). The divergence, time-mean vorticity tendency due to transients, and the zonal mean flow are specified from the GCM, and the deviation of the streamfunction from its zonal mean at an upper-tropospheric level is predicted. Nonlinear steady-state models suggest that the extratropical wave train is primarily forced from the central rather than the western Pacific and that subtropical divergence anomalies are of more importance than tropical anomalies. These nonlinear solutions can be reproduced with little loss in accuracy by linearizing about the zonally asymmetric climatological flow. If one linearizes about the zonally symmetric flow, the part of the solution forced from the western Pacific deteriorates significantly. The solution in the tropics and subtropics also deteriorates if advection of vorticity by the divergent flow is omitted.

Forcing by transients plays a secondary role in generating the extratropical wave train in these barotropic models, but it is pointed out that the subtropical convergence that forces the bulk of this wave train could itself be closely related to anomalies in the transient forcing.

Transients and the Extratropical Response to El Niño

ISAAC M. HELD

Geophysical Fluid Dynamics Laboratory, Princeton University, Princeton, New Jersey

STEVEN W. LYONS

Department of Meteorology Texas A & M University, College Station, Texas

SUMANT NIGAM

Center for the Study of Ocean–Land–Atmosphere Interactions, Department of Meteorology, University of Maryland, College Park, Maryland

(Manuscript received 11 April 1988, in final form 2 August 1988)

ABSTRACT

A baroclinic stationary wave model linearized about a zonally symmetric flow is used to interpret the extratropical atmospheric response to El Niño produced by a general circulation model. When forced by the anomalous diabatic heating and tendency due to transients, the linear model provides a useful simulation of this response. The direct response to anomalous diabatic heating is found to be small in the extratropics; the dominant term is the response to the anomalous transients, particularly the anomalous upper tropospheric transients in the vorticity equation. These results are complementary to those obtained with a nonlinear barotropic model by Held and Kang, and indicate that the anomalous subtropical convergence which plays a key role in that study is itself primarily forced by the anomalous transients. One can distinguish between two distinct parts of the response of the transients to the tropical heating: the movement of the Pacific storm track associated with the anomalous extratropical wave train, and changes in the penetration of Rossby waves into the tropics resulting from the modified tropical winds.

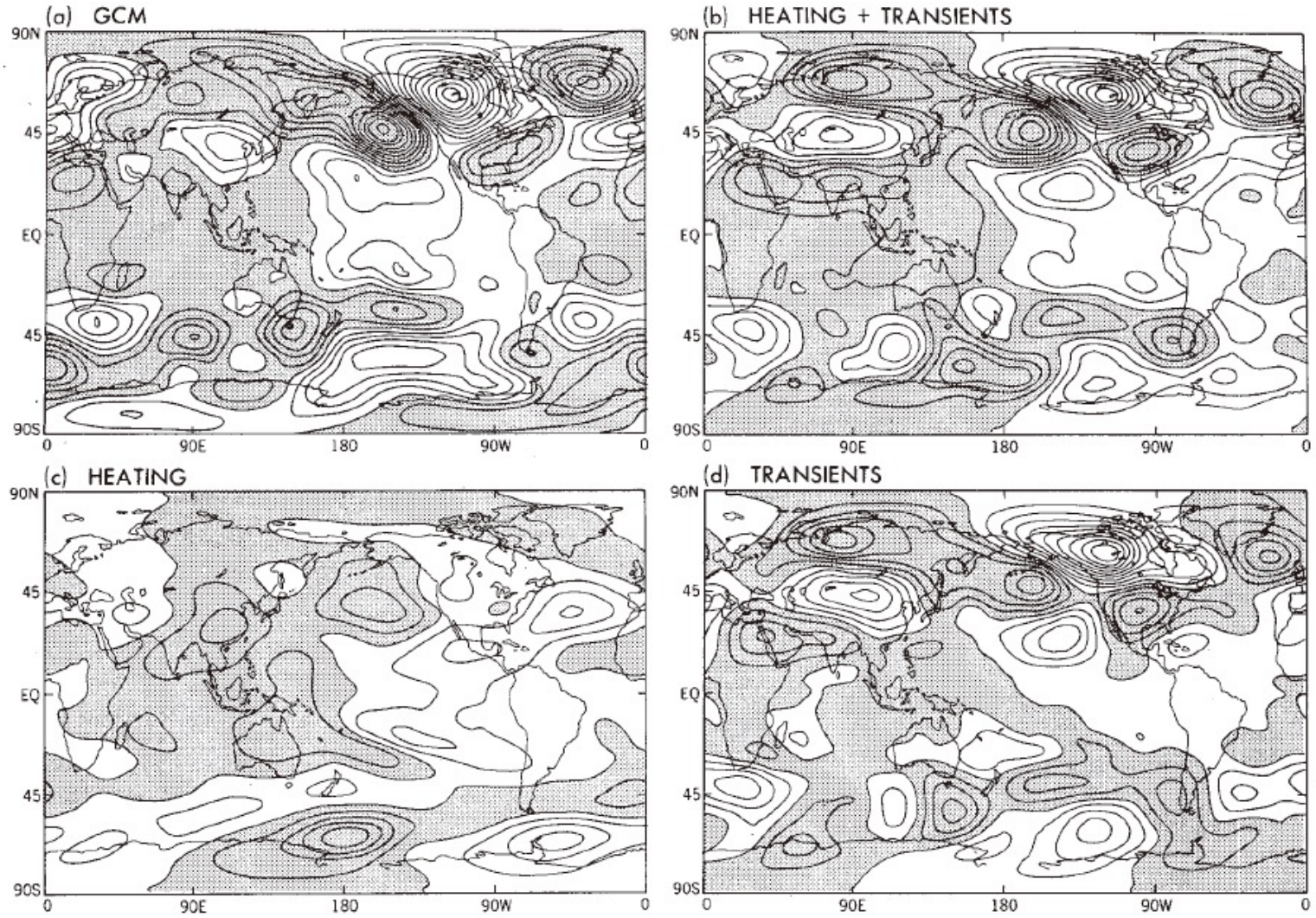

FIG. 1. (a) The 300 mb eddy geopotential height obtained from the GCM integration in Lau (1985) by compositing three El Niño winters and subtracting an analogous composite for three anti-El Niño winters; (b) the linear response of the 300 mb geopotential to the anomalous diabatic heating and forcing by transient eddies; (c) the linear response to anomalous diabatic heating; (d) the linear response to the anomalous forcing by transients. The contour interval is 10 m. Negative values are shaded.

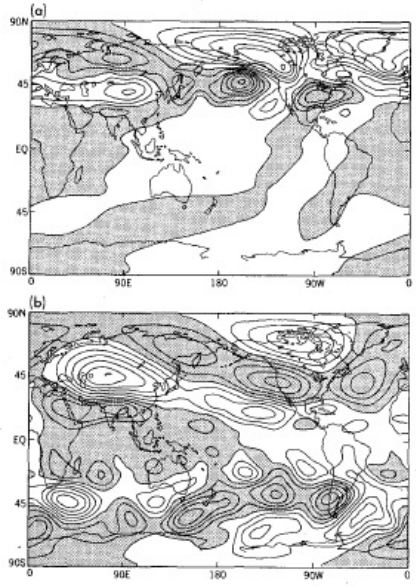

FIG. 5. The linear response of 300 mb geopotential height to the upper tropospheric anomalous vorticity tendency due to transients (a) between 25° and 70°N, and (b) south of 25°N. The contour interval is 5 m.

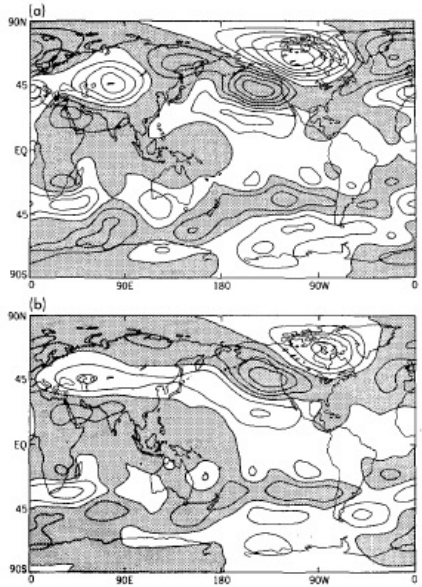

FIG. 6. The linear response of 300 mb geopotential height to the anomalous vorticity tendency due to transients near 200 mb, with the transient forcing computed in two different ways: (a) The vorticity tendency due to transients is computed as a residual from the GCM's seasonal mean σ-coordinate vorticity equation. (b) The difference between σ- and p-coordinate vorticity is ignored, and the anomalous transient eddy vorticity flux convergence at 200 mb, computed by sampling the GCM data once daily and interpolating to 200 mb, is substituted into the linear model at this same σ-level. Contour interval is 5 m.

sistent with the fact that a larger fraction of the response to low-latitude forcing is being captured at this level (cf. Fig. 5b). When we decompose Fig. 6a into the response to low- and midlatitude forcing, the low-latitude part is found to be much more dominant than in Fig. 5.

We have taken the GCM data, sampled daily and interpolated to 200 mb, and computed the convergence of the transient eddy vorticity flux, $\nabla \cdot (\overline{\mathbf{v}'\zeta'})$ in pressure coordinates. This quantity is calculated for each winter separately, and then composited over the El Niño and anti-El Niño cases. The difference between these two composites is used to force the linear model at σ-level 3. The result is shown in Fig. 6b. The pattern of the response is very similar to that in Fig. 6a, but the amplitude is smaller. The difference between these two figures must be due to the neglect of vertical advection and twisting in 6b, differences between σ- and p-coordinate vorticity, or interpolation and sampling errors.

Figure 7 is the anomalous streamfunction tendency,

$$-\nabla^{-2}[\nabla \cdot (\overline{\mathbf{v}'\zeta'})] \qquad (1)$$

obtained from the explicitly computed vorticity fluxes

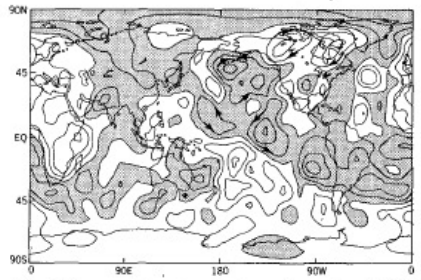

FIG. 7. The anomalous streamfunction tendency due to the 200 mb transients computed explicitly from the GCM data sampled daily and interpolated to 200 mb. Contour interval is 10 $m^2 s^{-2}$. Positive values are shaded.

Kang et al. (2011, CD)
Impact of transient eddies on extratropical seasonal-mean predictability in DEMETER models

Climatology of Transient eddy activity $\overline{\psi'^2}^c$

Using 2-8 day filtered streamfunction (ψ') [m^2s^{-1}]

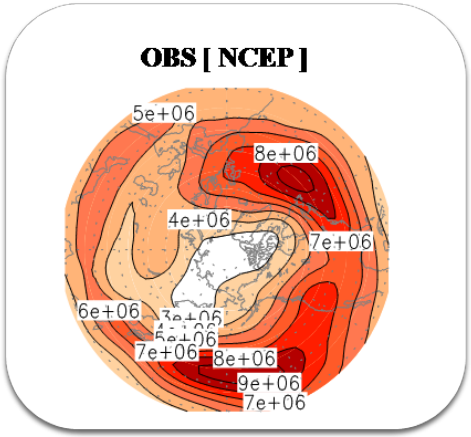

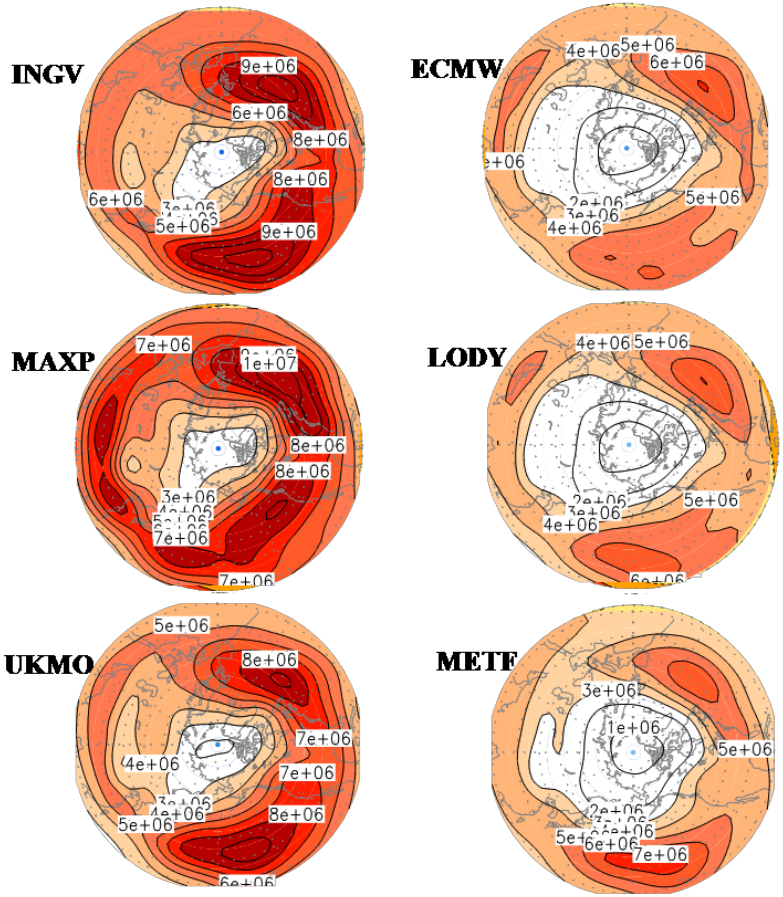

El Nino period (82/83, 91/92, and 97/98) - La Nina period (88/89, 98/99, and 99/00)

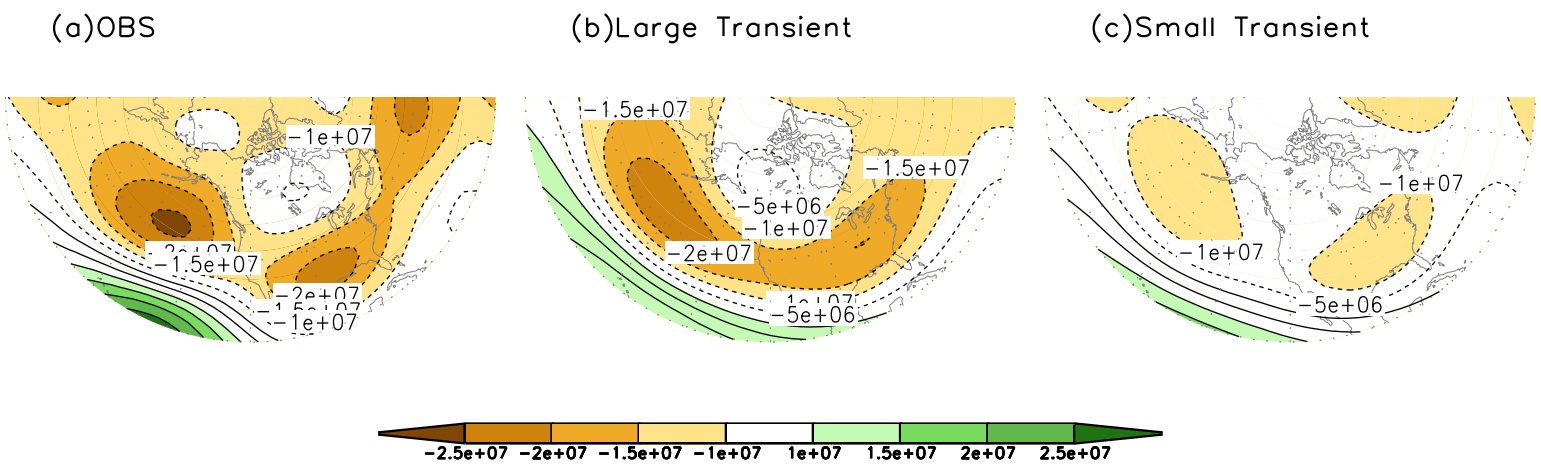

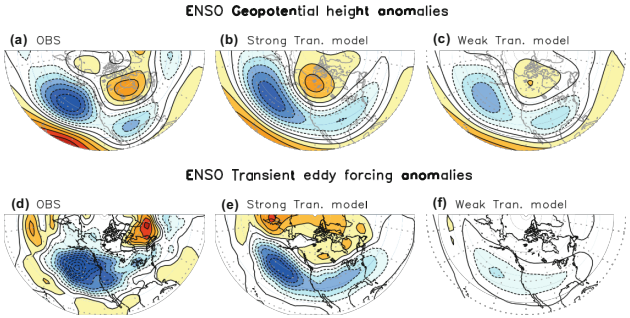

Fig. 6 ENSO anomalies of the 200-hPa geopotential height, a the observations, b the composite of strong transient models, and c of the weak transient models. d, e, f are as a, b, c except for transient eddy forcing. ENSO anomaly is defined by the El Nino composite minus the La Nina composite. The contour intervals are 30 m for 200-hPa geopotential height and 5 9 10^{-5} m s^{-1} for transient eddy forcing

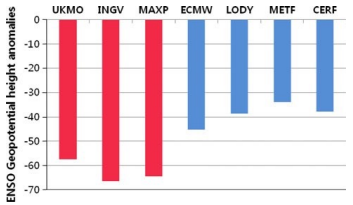

Fig. 7 Magnitude of 200-hPa geopotential height anomalies associatd with ENSO averaged over 25°N–60°N, 150°E–120°W. *Red* (*Blue*) *bar* represents strong(weak) transient models

during ENSO; however, a part of the extratropical circulation anomalies are excited directly by tropical forcing through the teleconnection mechanism (Horel and Wallace 1981; Hoskins and Karoly 1981) and transient anomalies associated with the jet stream changes also play an important role in the PNA circulation anomalies (Held et al. 1989; Jin et al. 2006a). The intensity of transient forcing to the seasonal-mean circulation can be roughly estimated by the parameter c in Eq. (2) as below.

$$c(t) = \frac{\int \overline{\phi_{\mathrm{reg}}}^{a}(x,y) \times \left(\frac{\partial \overline{\phi'}}{\partial t}\right)_{\mathrm{tr}}(x,y,z)\,dx\,dy}{\int \left[\overline{\phi_{\mathrm{reg}}}^{a}(x,y)\right]^{2} dx\,dy} \qquad (2)$$

where / reg ðx; yÞ is geopotential height pattern regressed with PNA index over the domain of 150°E–60°W and

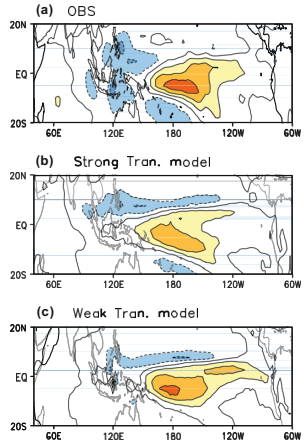

Fig. 8 As in Fig. 6 except for precipitation anomaly. The contour interval is 4 mm day^{-1} and the *shading* denotes values greater than - 6 mm day^{-1} and less than 6 mm day^{-1}

30°N–70°N. The parameter c denotes the strength of transient forcing, which is estimated with the model data. Figure 9 shows the distribution of c (y-axes) for different

Abid, Kang, Mansour, Kucharski (2015, CD)

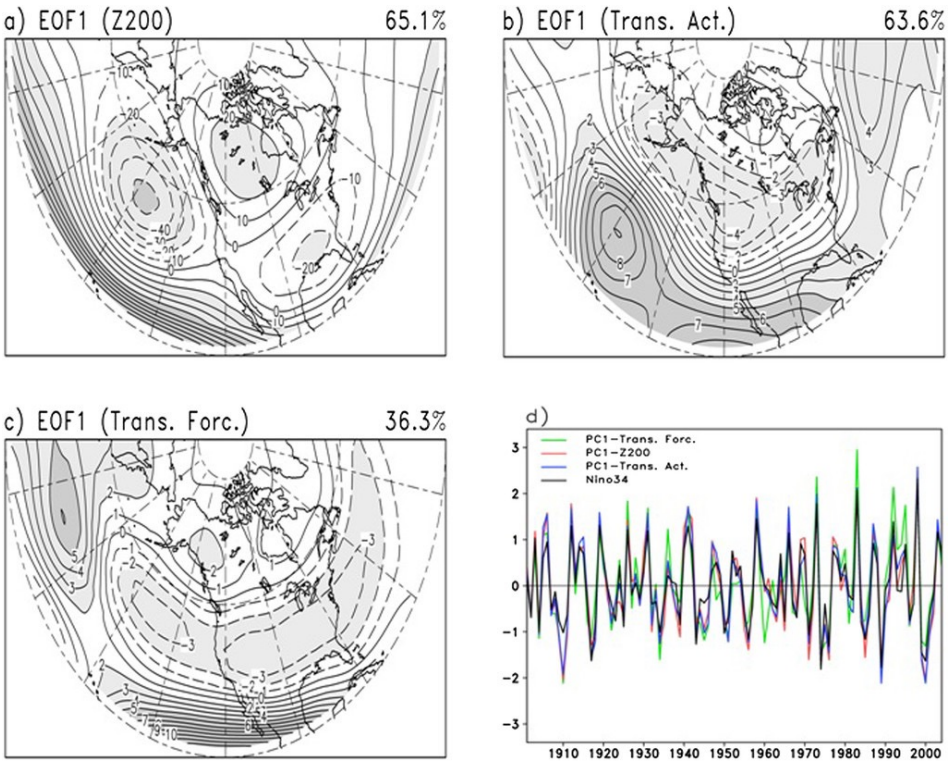

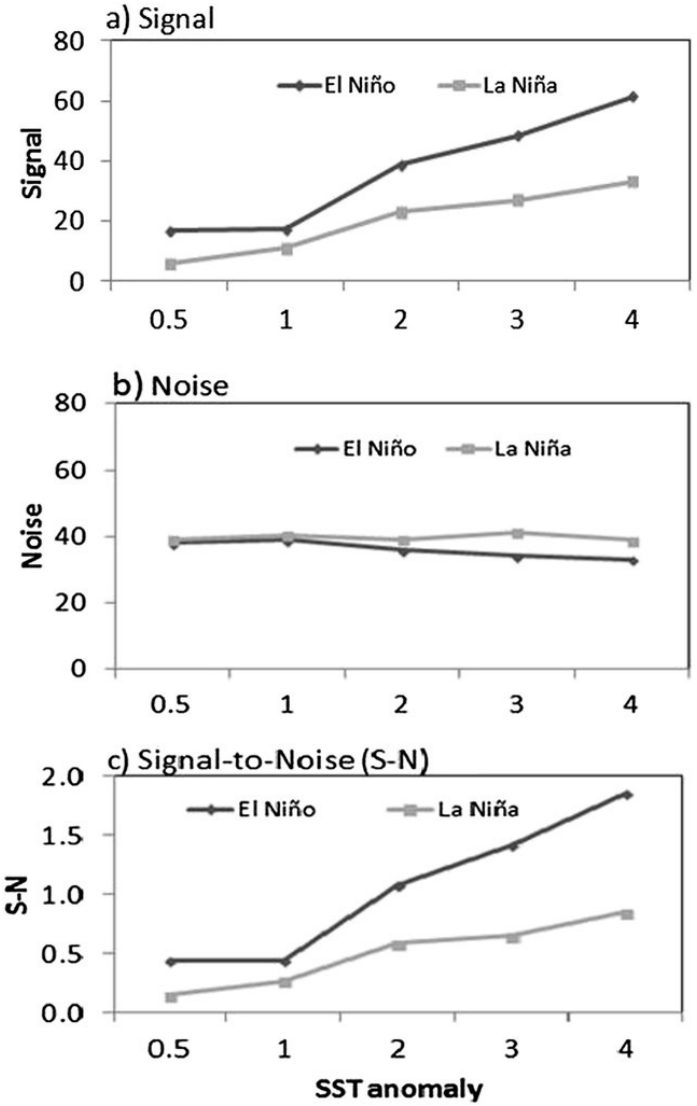

Stratosphere Memory influencing tropospheric anomalies

Stratospheric Influence on Predictability Enhancement in Late Winter

Prediction skill change with lead time

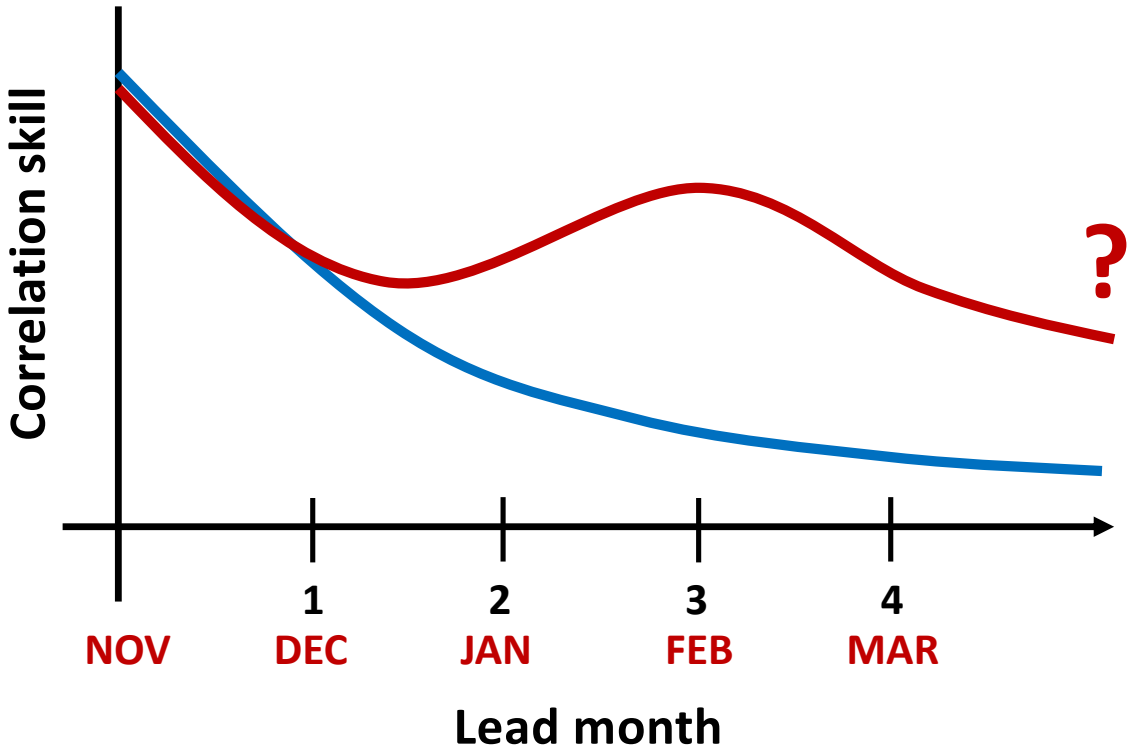

Monthly-mean correlation skill of PNA index for 1-3 lead months
(starting from November)

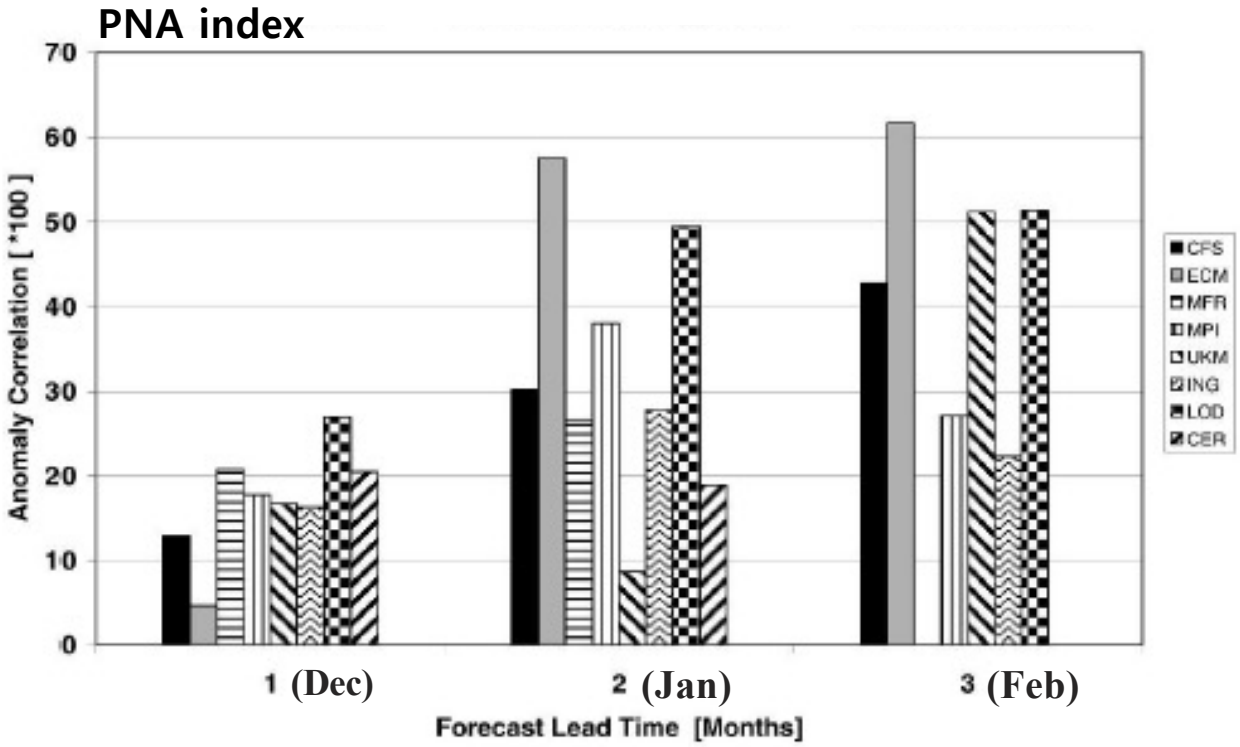

CFS and the seven models in the DEMETER project Johansson (2007)

Monthly-mean correlation skills for 1, 3, and 5 lead months

(starting from 1 November)

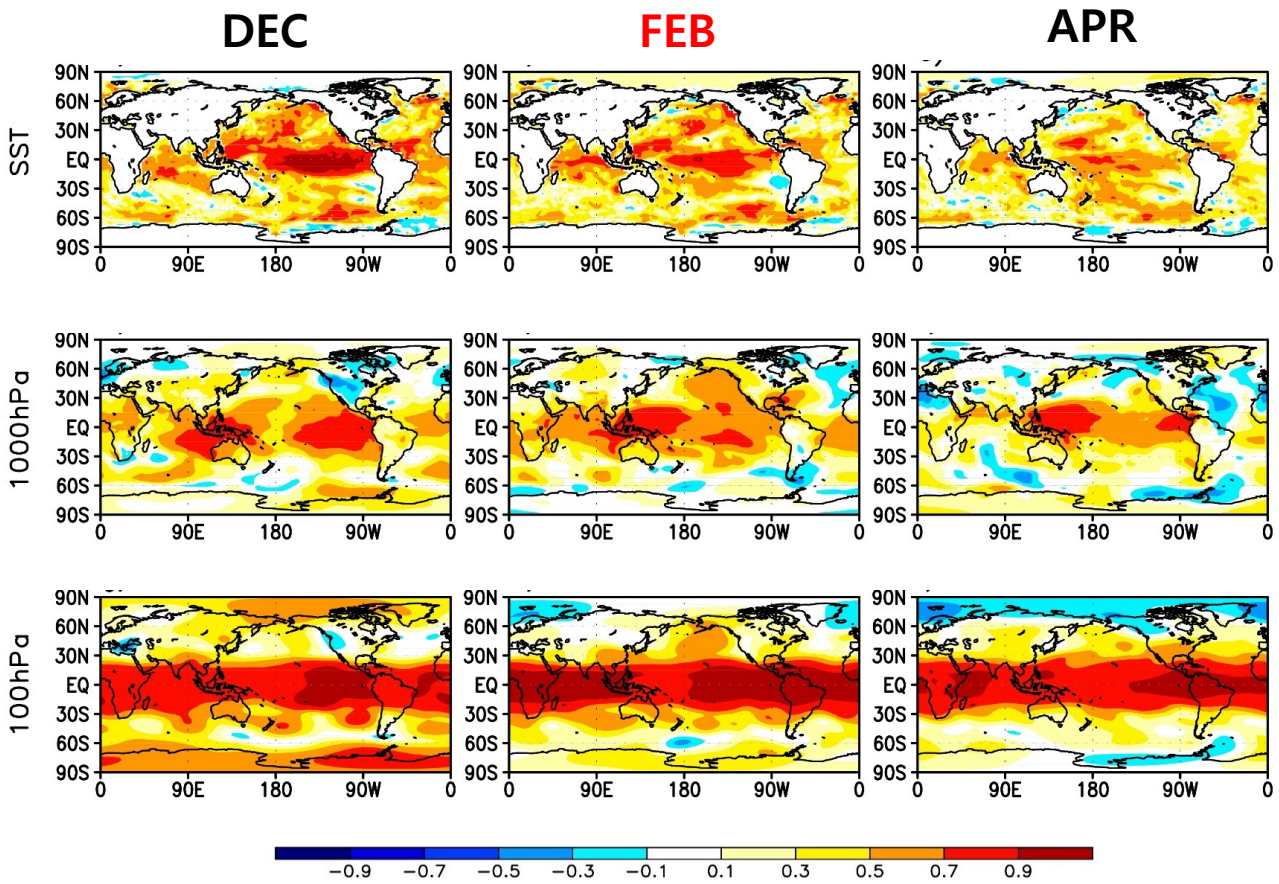

Stratospheric downward influence on prediction skill

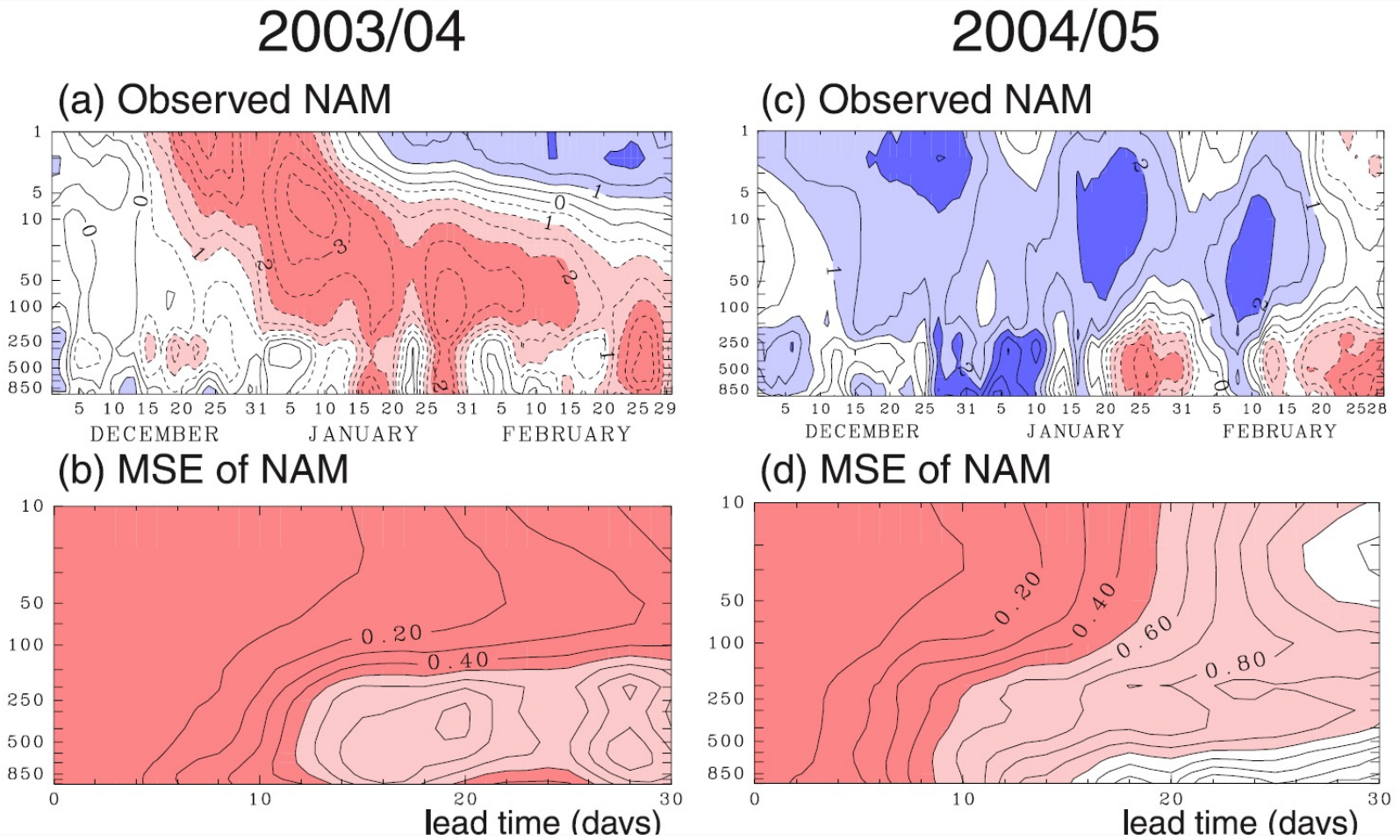

The mean square error (MSE) of the forecasts with negatively large 30-hPa NAM anomalies at the initial time is significantly smaller than that of the forecasts with positively large NAM anomalies for the lead time from 5 to 13 days.

Mukougawa et al. (2009)

PDF of area averaged zonal wind at 50hPa [0-360E, 55-65N]

Bin size = 0.2 std.

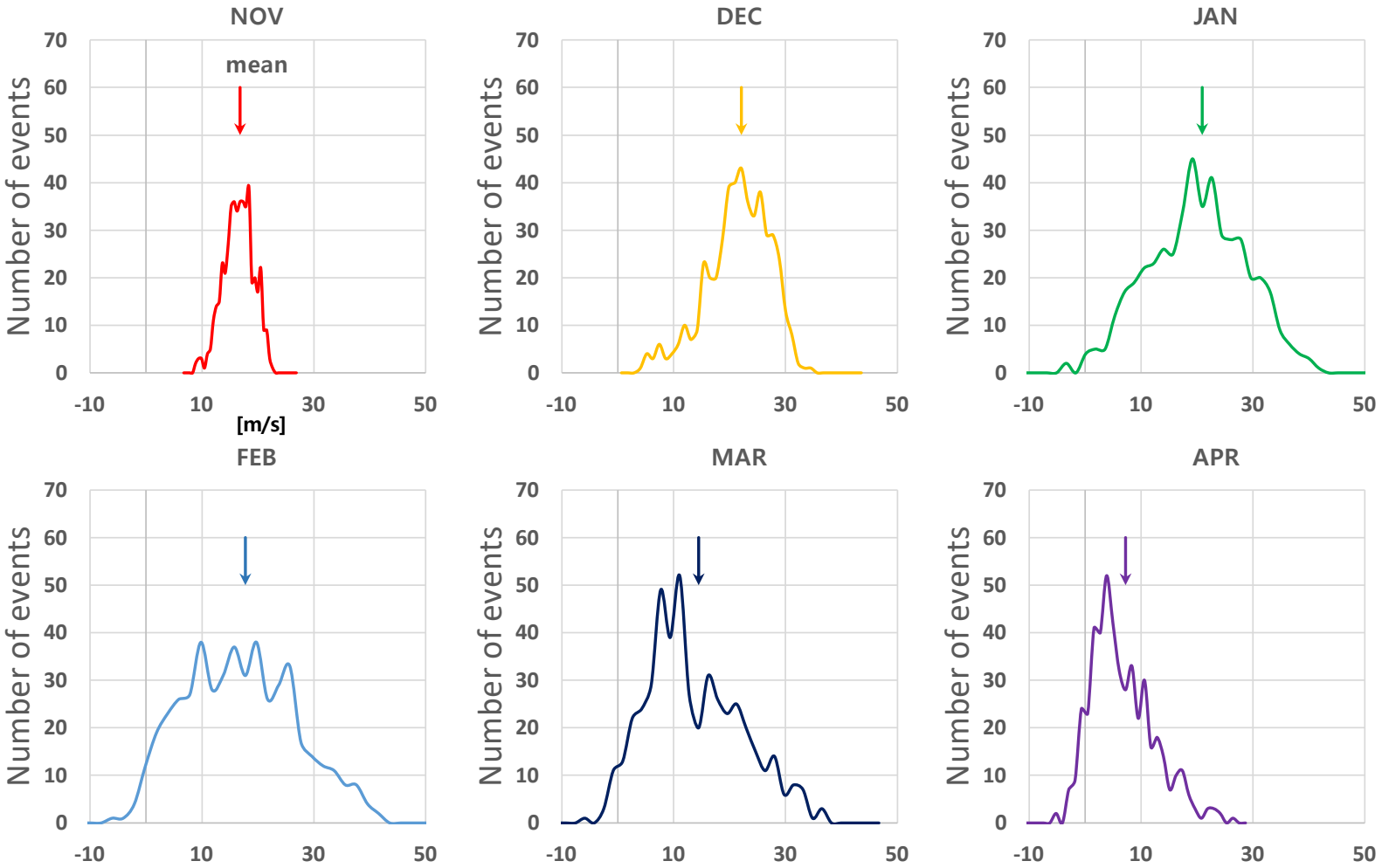

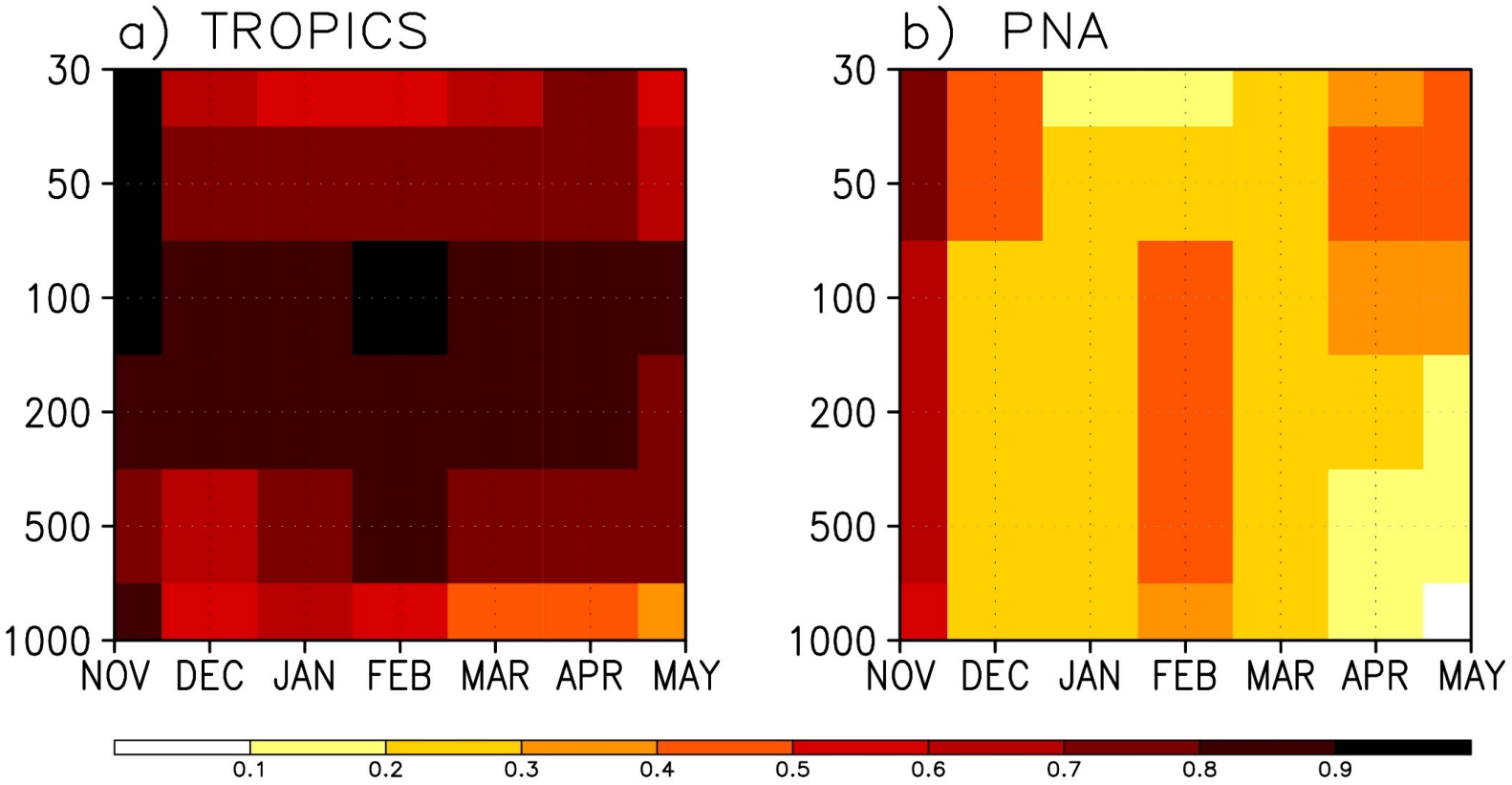

Fig. 2. Regional averages of correlation skills for geopotential heights from 1000 hPa to 30 hPa with lead times from 0 to 6 months. 0 and 6 months correspond to November and May, respectively. a) is for the average over the tropics between 20N and 20S, and b) for the Pacific-North American region of 20N-70N and 150E-60W.

Review of earlier papers

- Bjerknes (1966, 1969) “Teleconnection”

Intensification of westerly momentum associated with intensified Hadley circulation

- Hoskins and Karloy (1981) “Rossby Wave ray theory”
- Simmons et al. (1983) “Regional barotropic instability”
- Held et al. (1989) “Transient forcing”
- Stratospheric path way

Extratropical circulation modes

ENSO forced mode vs Internal mode

- Lau (1981) Climatological SST run for 15 yrs.
  Examination of Interannual variability (rms) of extratropical GH, similar magnitudes as observed.

- Kang and Lau (1986) observed SST run (AMIP)
  1^{st} EOF mode: ENSO mode, 2^{nd} EOF mode: internal mode

- Straus and Shukla (2002) Does ENSO force the PNA?
  ENSO mode could be different from the PNA mode

- External ENSO mode vs Internal mode?

Does ENSO Force the PNA?

DAVID M. STRAUS AND J. SHUKLA

Center for Ocean–Land–Atmosphere Studies, Calverton, Maryland

(Manuscript received 29 May 2001, in final form 21 February 2002)

ABSTRACT

The primary effect of El Niño–Southern Oscillation (ENSO) sea surface temperature (SST) anomalies is to force distinct midlatitude patterns, and not only to modify the probability of the internal variability patterns [such as the Pacific–North American (PNA) pattern of Wallace and Gutzler]. Both the spatial structure and probability distribution of the external ENSO pattern are distinct from the PNA pattern. Ensemble general circulation model (GCM) integrations for 30 winters have been analyzed in the Pacific–North America region. These winters span the recent period of 1981/82 through 1998/99, plus 12 earlier winters; the entire dataset includes six El Niño (warm) and seven La Niña (cold) events. The ensemble size is nine simulations. Empirical orthogonal function (EOF) analysis is carried out for all GCMs and observed seasonal means, for the GCM ensemble means, and for the GCM deviations about the ensemble means. EOF-1 of the GCM 200-hPa height (Z) ensemble mean agrees well with EOF-1 of all GCM seasonal means, and with the pattern that optimally filters out the internal variability. This ENSO pattern agrees with EOF-1 of reanalysis data, although the latter is modified in the Atlantic sector by the presence of the North Atlantic Oscillation pattern. An internal pattern closely resembling the PNA pattern is obtained here from reanalyses as EOF-2 of Z for 37 normal winters (winters that are neither warm nor cold). The GCM version of the PNA pattern can be seen in EOF-2 of the deviation of the GCM means about the ensemble mean, EOF-3 of all GCM seasonal means, and EOF-2 of a GCM integration made with climatologically varying SST.

Projections of all GCM seasonal means in a low-dimensional space indicate a segregation of the warm winter seasonal means from those of normal winters along the axis representing the external pattern. There is no support for the hypothesis that the probability distribution functions (pdfs) of internal and external variability are similar.

There is clear evidence of shifts in the probability of occurrence of internal patterns in warm and cold winters compared to normal winters. This has been analyzed in terms of only one set of characteristic patterns based on all winters. A more detailed investigation of the dependence of internal variability on SST forcing requires a larger ensemble size.

Intraseasonal variability is examined by projecting all individual pentad means on both the ENSO pattern and the PNA pattern (represented by the EOF-1 and EOF-3 of all seasonal means). For five out of the six warm winters, the pdfs of the time series of the coefficient of the ENSO pattern are shifted significantly toward more positive values, with very little probability of having a negative coefficient. For the cold events, the ENSO pattern has greater variability than the PNA pattern. The pdf of the projections of pentads on the seasonal mean anomaly for the same year are sharply peaked.

The GCM tropical heating maps show similar patterns for cold and normal winters, while the warm winter pattern is clearly different, especially along the equator. The heating anomalies have larger magnitude in warm than in cold winters. Linearity of the leading ensemble mean principal component (PC) with respect to the Niño-3 index of SST is seen only for positive SST anomalies. When Niño-3 is replaced by heating averaged over the central Pacific, there is a consistent relationship between the ENSO PCs and both positive and negative heating. Niño-3 depends on heating in a linear way for positive heating anomalies, but is independent of heating for negative anomalies.

EOF Patterns of Z200 in PNA region [1981-2014 DJF]

ERA-interim

AMIP

CLIM

AMIP
(exclude ENSO years)

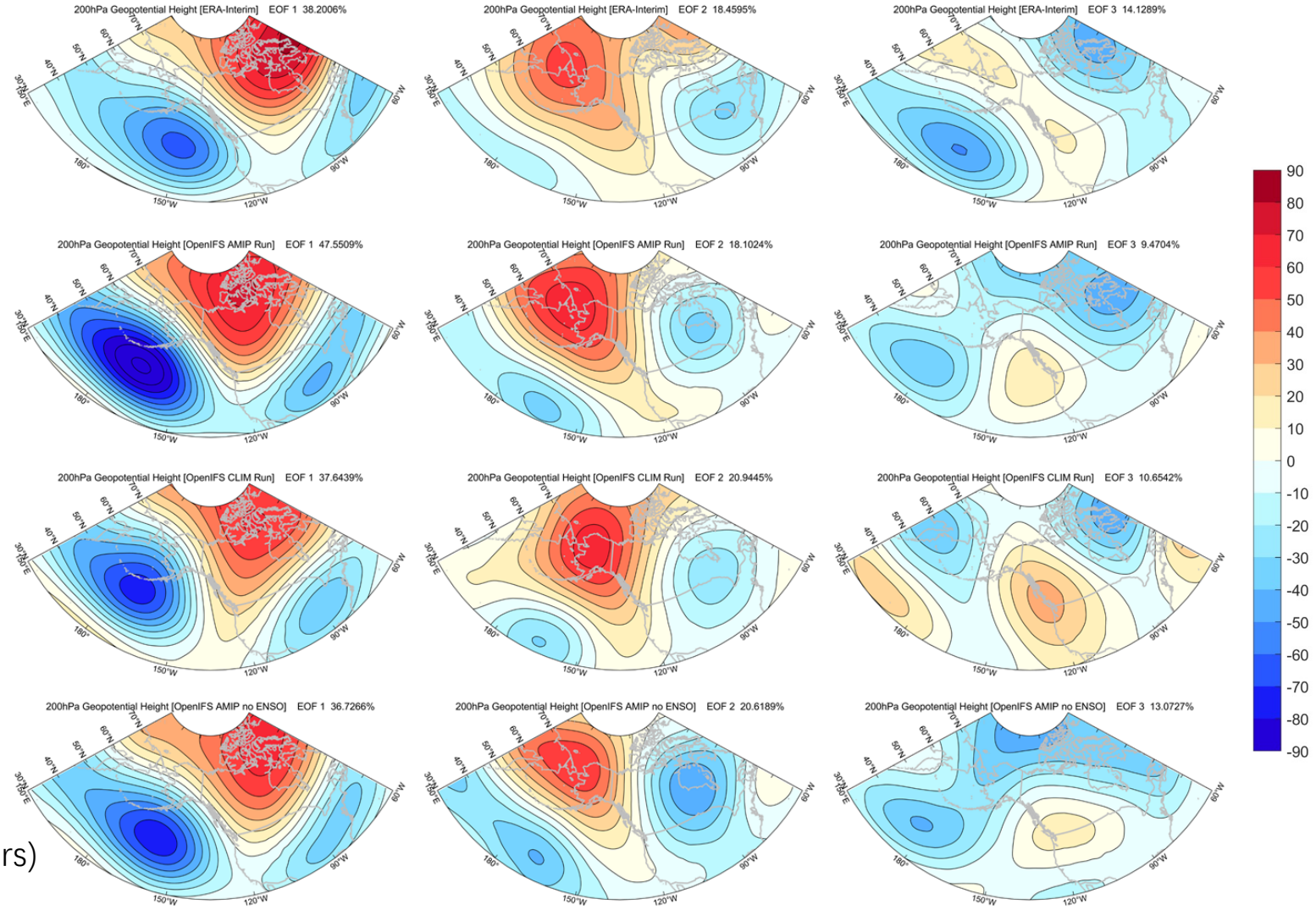

Correlation Coefficients with PNA PCs (Rainfall)

AMIP-PC1

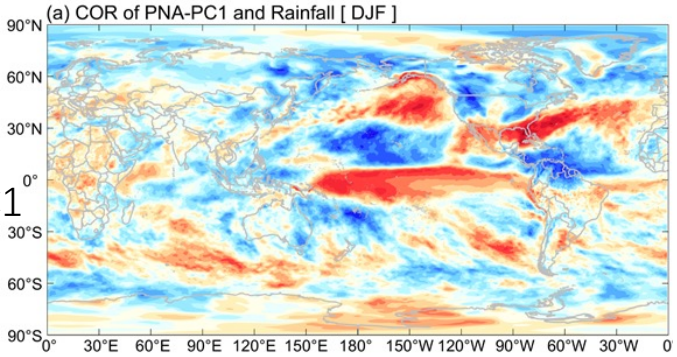

CLIM-PC1

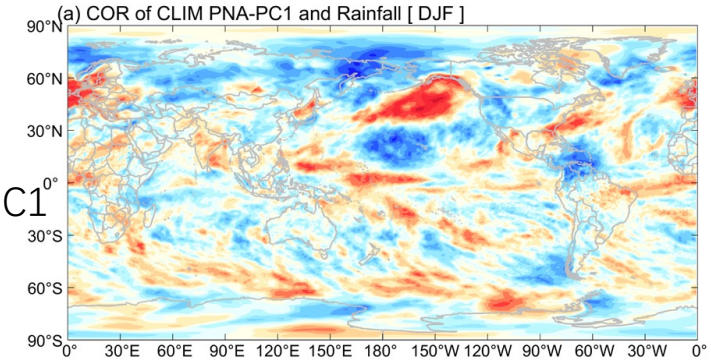

AMIP-PC2

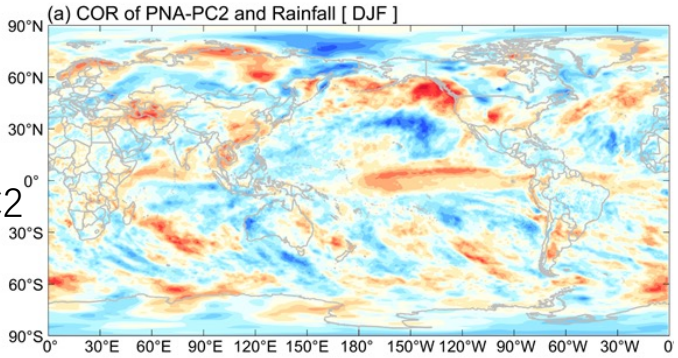

CLIM-PC2

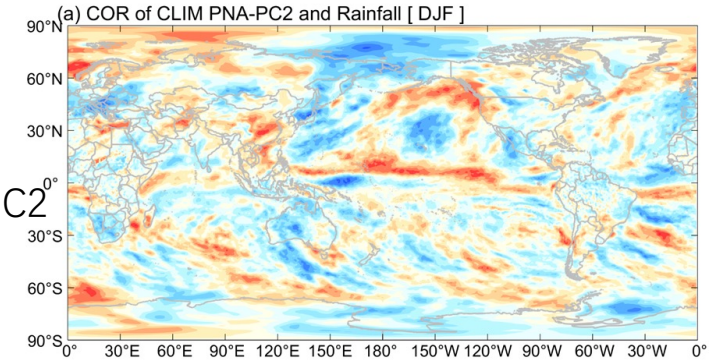

AMIP-PC3

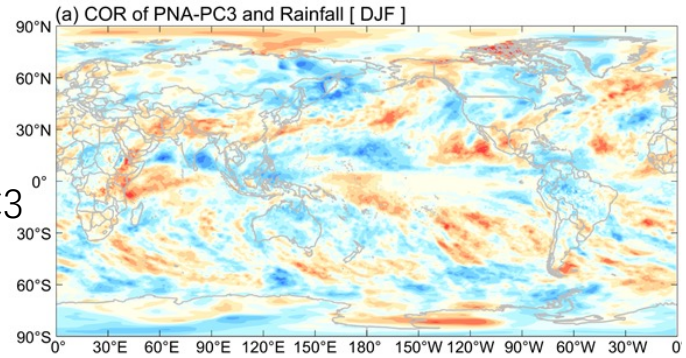

CLIM-PC3

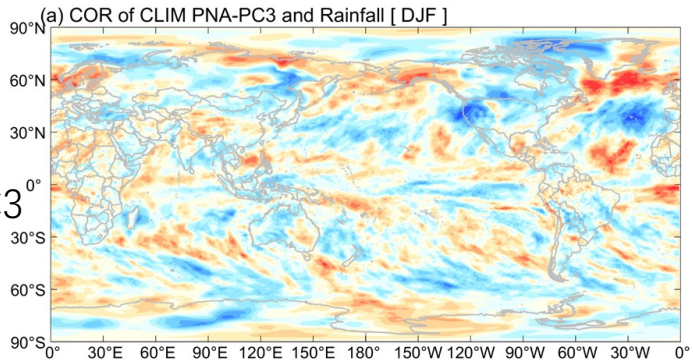

Although no ENSO impact, the convection signal from central Pacific still exist. But the correlation over North America is much weaker.

Correlation between PNA-PCs and Transient eddy forcing

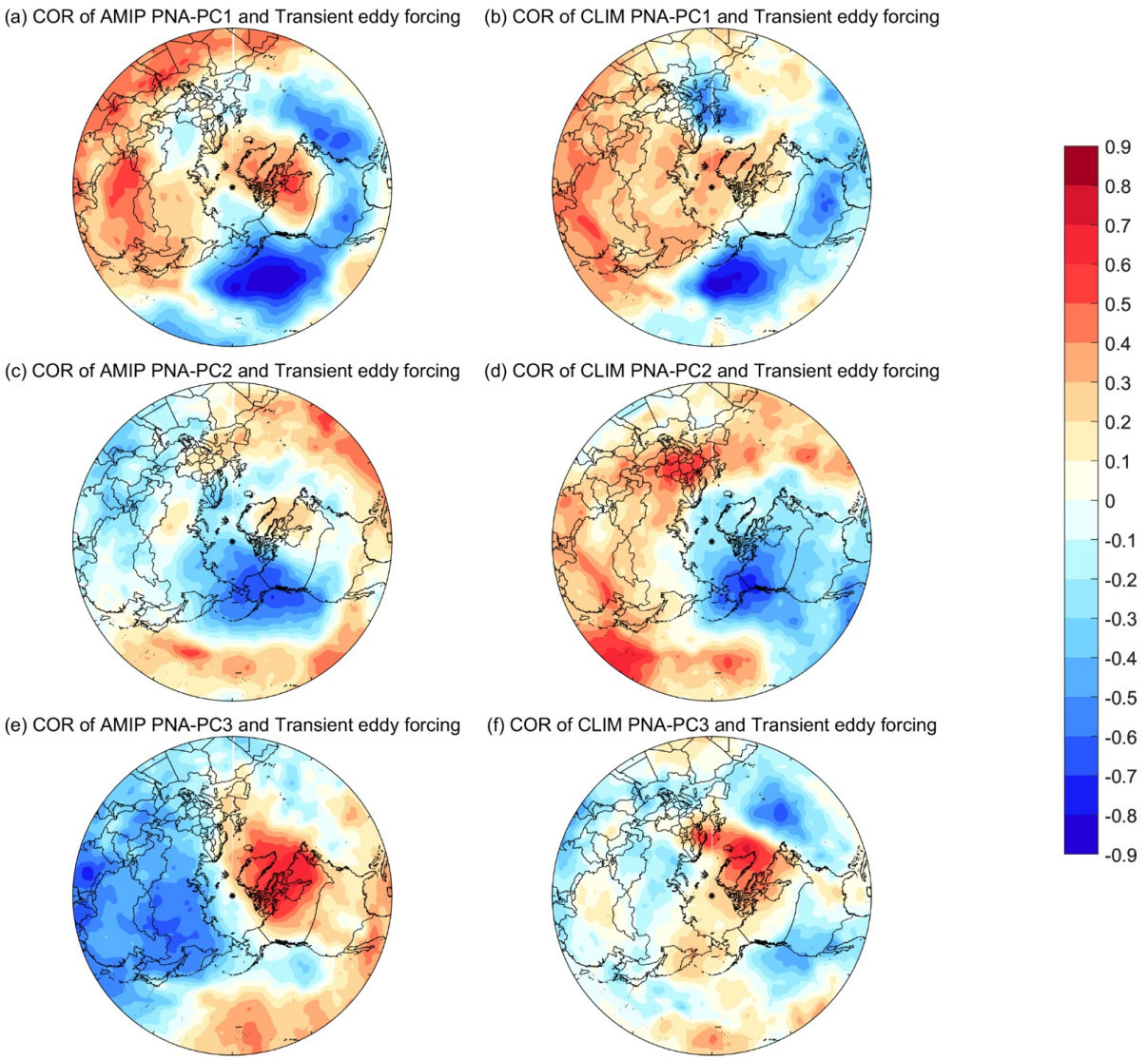

Internal and ENSO-forced PNA modes (ICTP Speedy model)

ENSO-forced pattern (Nino 3.4)

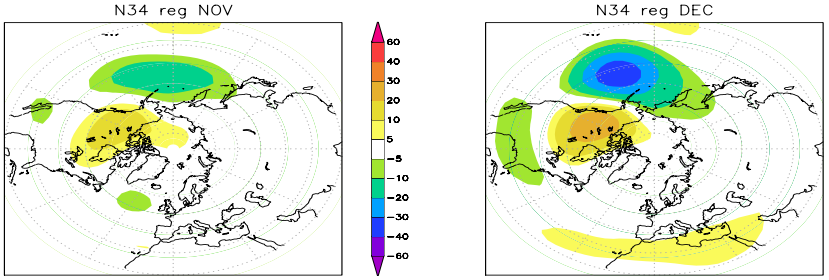

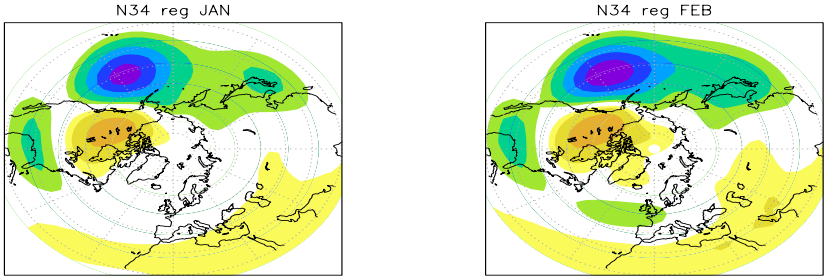

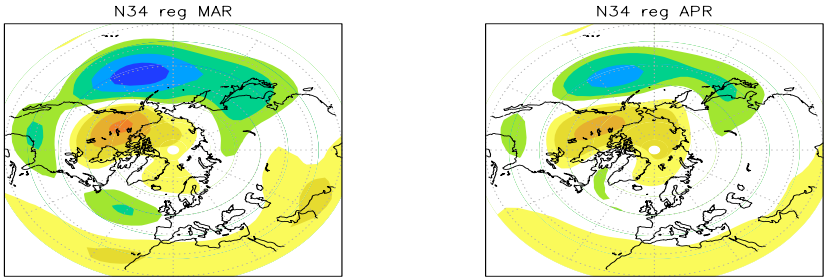

Internal mode (EOF of Clim simulation)

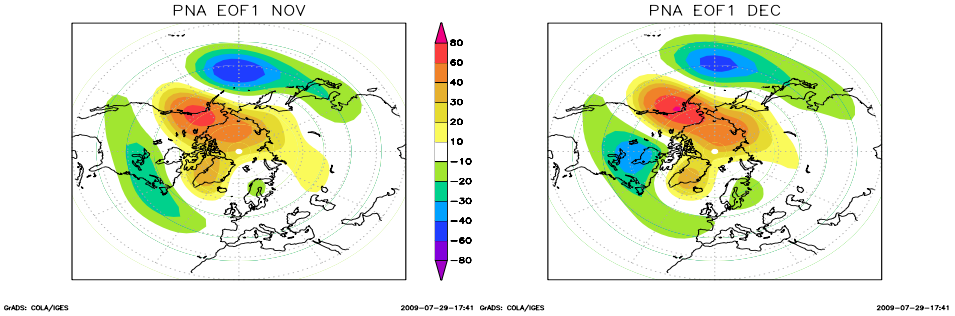

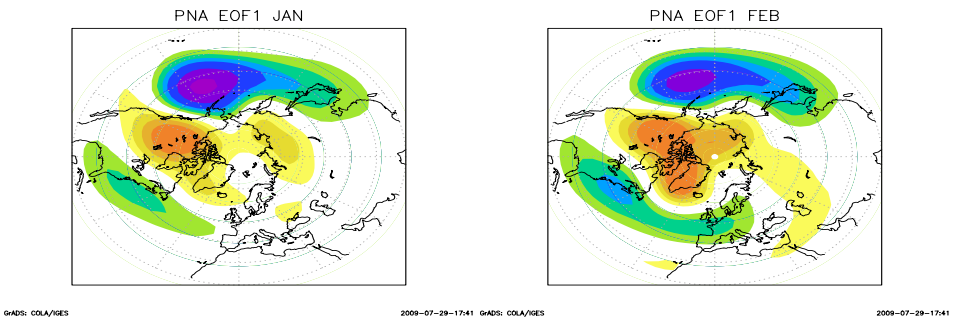

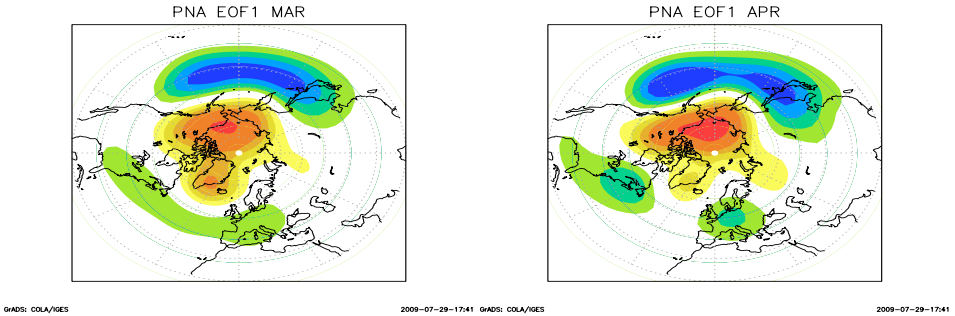

ENSO vs Internal modes

Model dependent ??

Resolution dependent?

Transients

➢ Dependency of model resolution

- 3 hourly precipitation

300km resolution

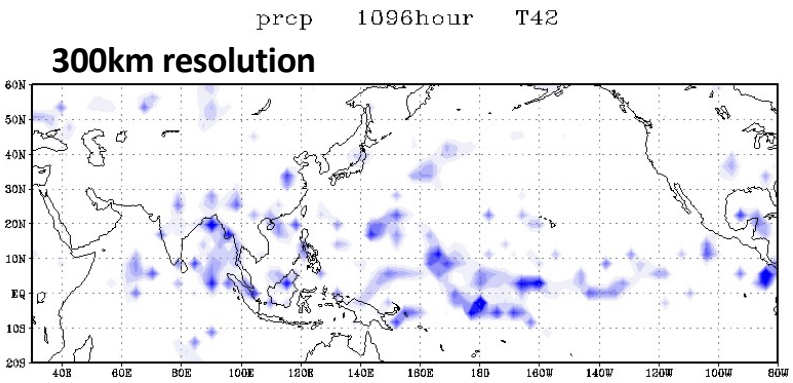

125km resolution

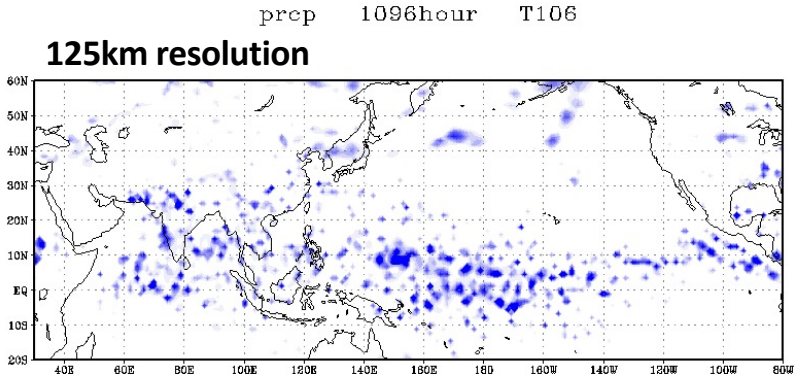

25km resolution

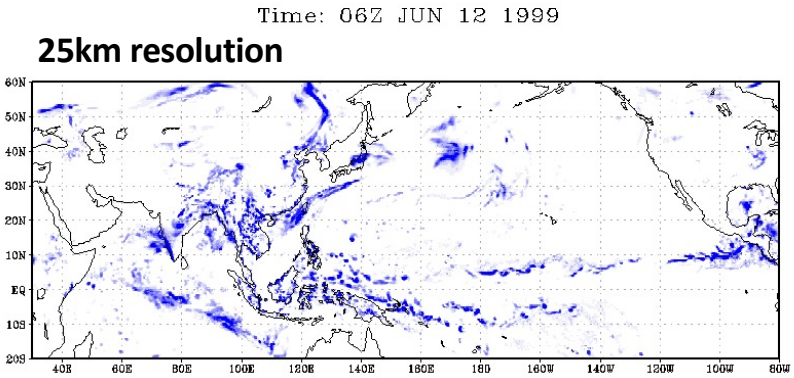

Very High resolution GCM simulation – 25km resolution

- 1997 JJA (El Nino) – 1999 JJA (La Nina)

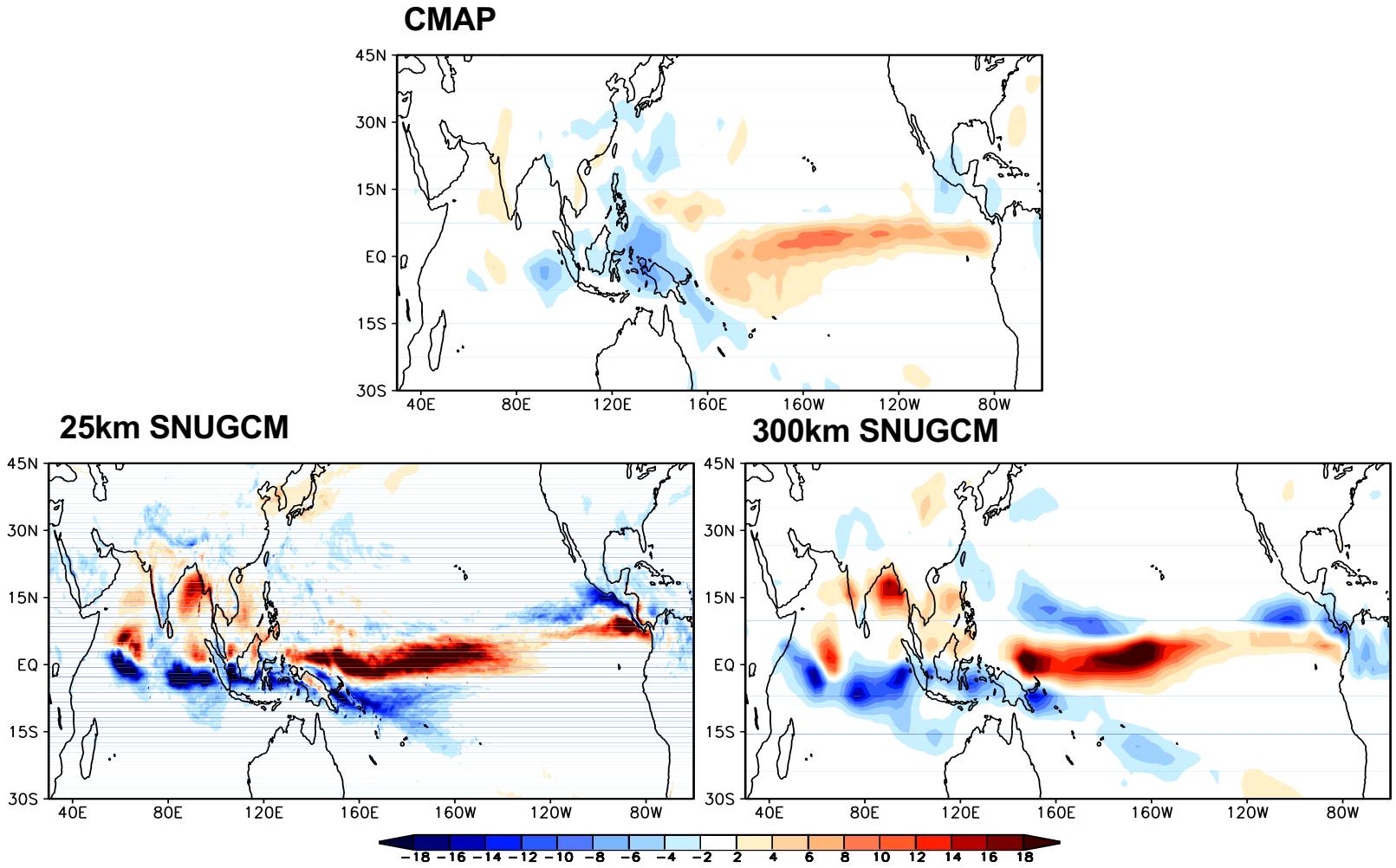

Very High resolution GCM simulation – 25km resolution

- The 200 hPa streamfunction : 1997 El Nino case – 1999 La Nina case (Difference)

NCEP

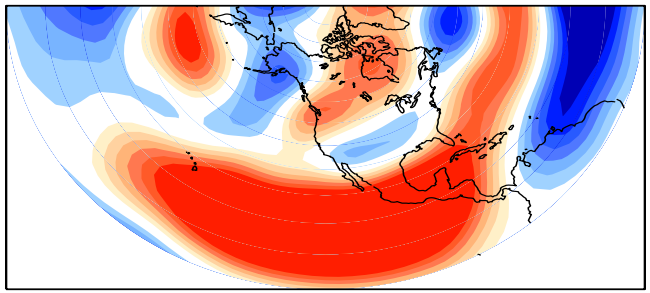

25km SNUGCM

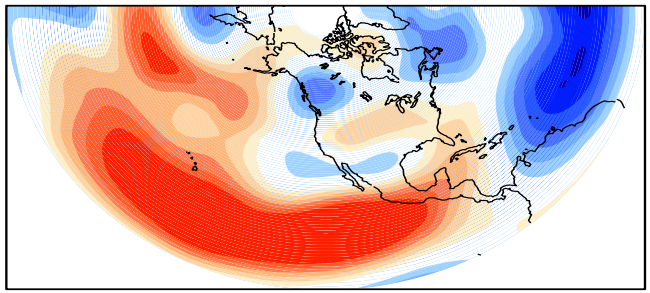

300km SNUGCM

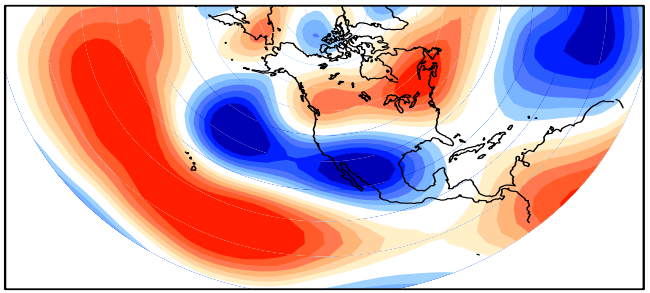

Perturbation from the zonal mean & seasonal mean

High Frequency eddy activity $\overline{u'^2}$

- 1997 El Nino case

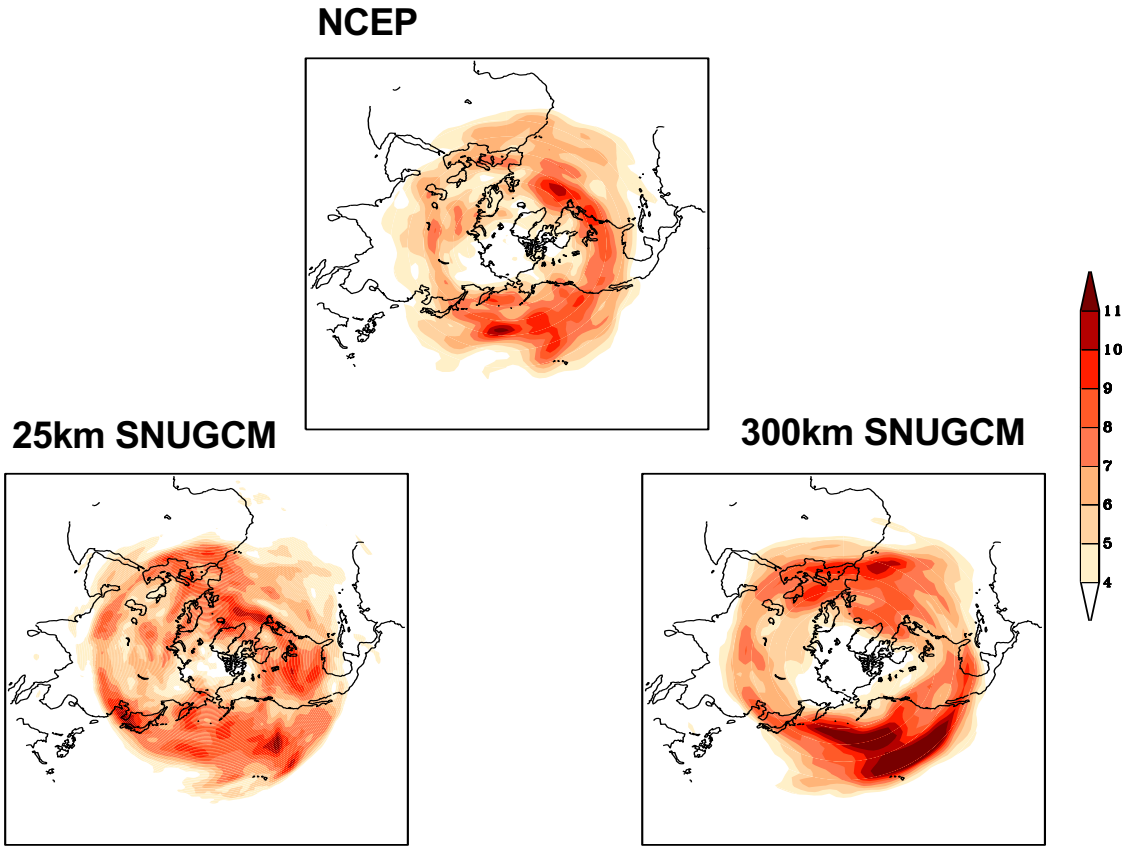

The standard deviation of 2~8 day filtered 200hPa zonal wind

Transient eddy forcing

✓ 6-ensemble mean

- 1997 El Nino case (JJA mean) – 200 hPa filtered zonal/meridional wind

NCEP

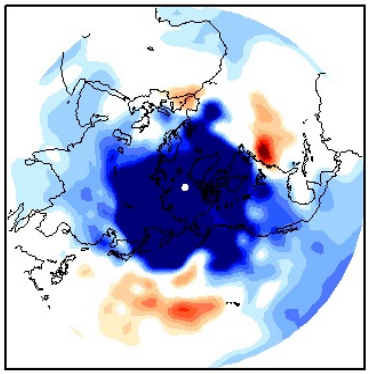

Using quaisi-geostropic approximation,

$$\frac{\partial \overline{\psi}}{\partial t} = -\nabla^{-2}[\nabla \cdot (\overline{V'\zeta'})]$$

25km SNUGCM

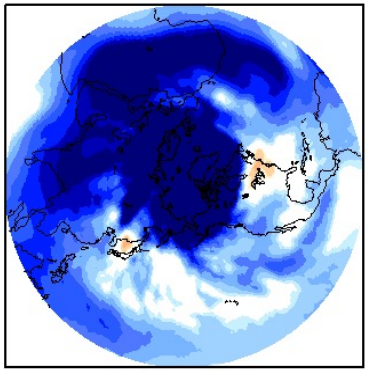

125km SNUGCM

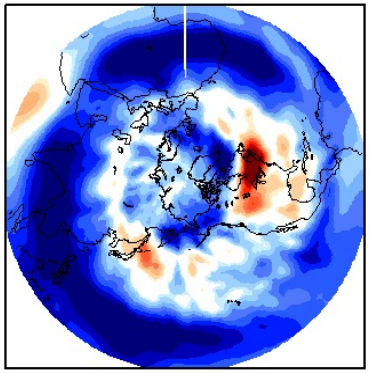

300km SNUGCM

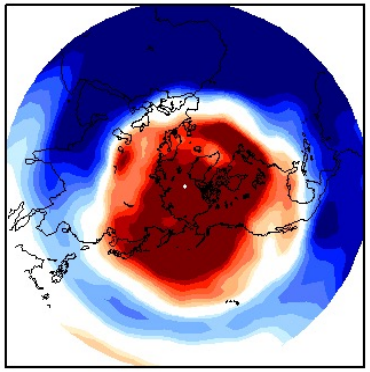

Summary

- Reviewed the earlier papers, provided an original concept and theory for the extratropical teleconnection associated with ENSO.
- Still question on the internal vs forced modes
- Resolution dependency on the teleconnection simulation

Covariance map of normalized monthly-mean 100hPa GPH anomaly

(Starting from 1 Nov.)

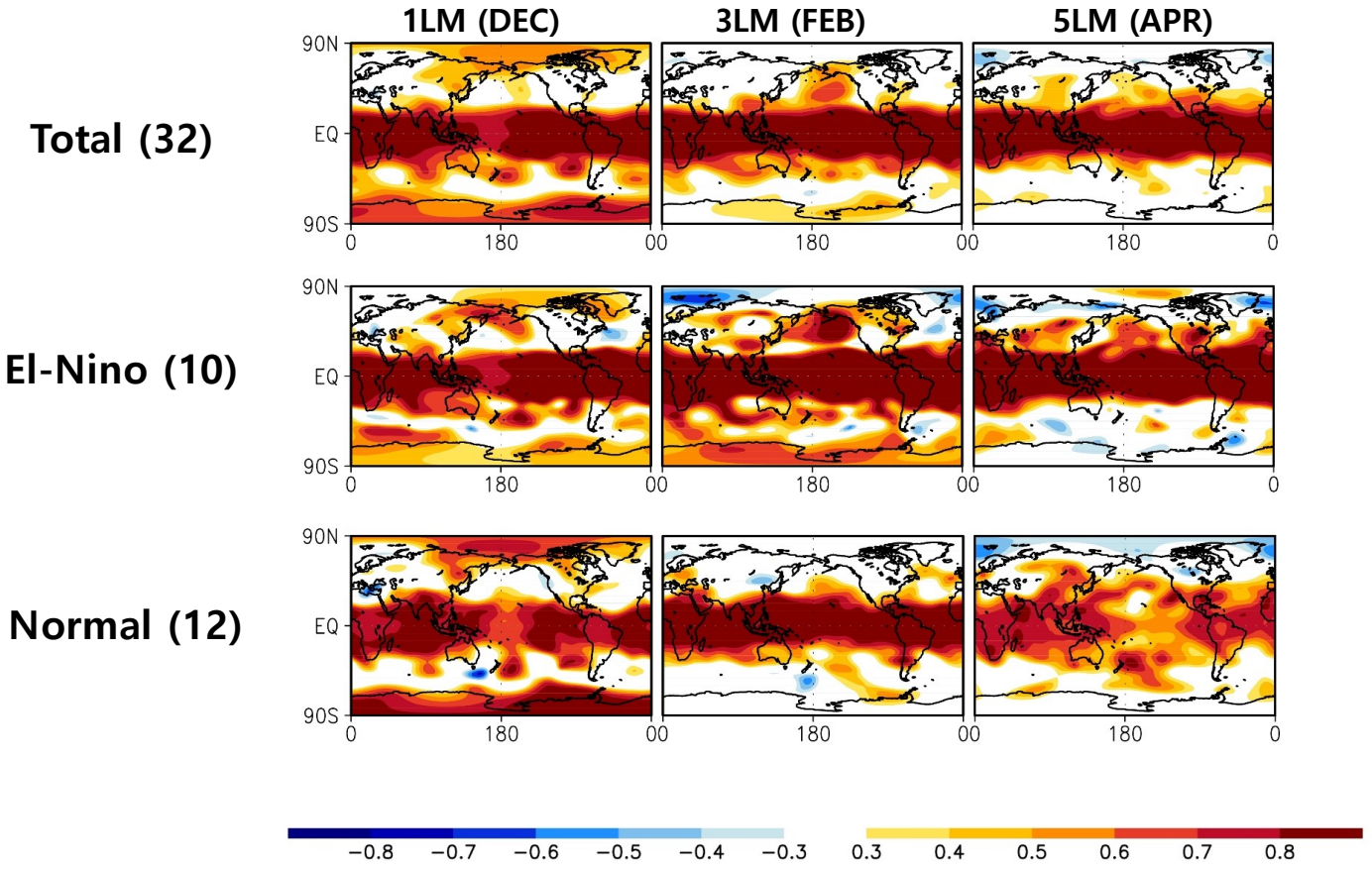

A Possible Mechanism of Stratospheric downward influence

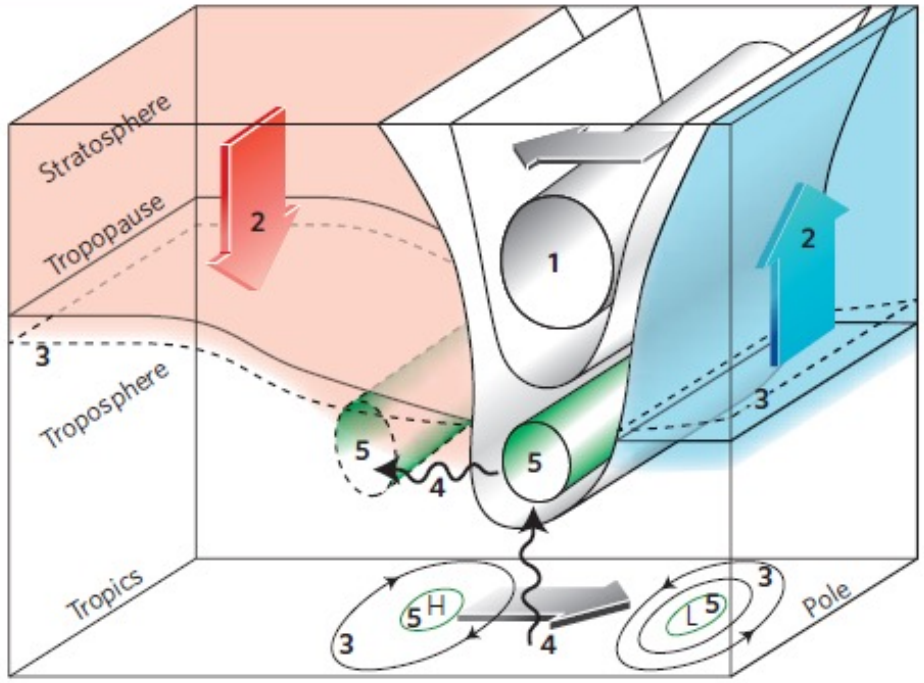

(1) Wave-driving ⟶ Changes in the speed of the stratospheric jet

(2) Return flow within the planetary boundary layer for the anomalous circulation

(3) Increase of the tropopause height & Decrease of mean SLP in polar latitudes and vice versa in mid-latitudes

(4) Tropospheric eddy feedbacks

(5) Poleward shift of the tropospheric jet

Kidston et al. (2015)